Estonian Journal of Earth Sciences
2025, **74**, 1, 34–52

https://doi.org/10.3176/earth.2025.03

www.eap.ee/earthsciences
Estonian Academy Publishers

RESEARCH ARTICLE

Received 24 April 2024
Accepted 27 June 2024
Available online 13 January 2025

Keywords:
geology, Paleoproterozoic, volcanic arc, zircon age, titanite age, compression, extension

Corresponding author:
Teemu Vehkamäki
tetave@utu.fi

Citation:
Toivanen, E., Vehkamäki, T., Väisänen, M., Kara, J. and O'Brien, H. 2025. Geochronology of the felsic rocks in Orijärvi, southern Finland – implications for stratigraphy. *Estonian Journal of Earth Sciences*, **74**(1), 34–52. https://doi.org/10.3176/earth.2025.03

Geochronology of the felsic rocks in Orijärvi, southern Finland – implications for stratigraphy

Elisa Toivanen[a], Teemu Vehkamäki[a], Markku Väisänen[a], Jaakko Kara[a] and Hugh O'Brien[b]

[a] Department of Geography and Geology, University of Turku, Akatemiankatu 1, FI-20014 Turku, Finland

[b] Geological Survey of Finland, Vuorimiehentie 5, FI-02151 Espoo, Finland

ABSTRACT

The Orijärvi area within the Paleoproterozoic Uusimaa belt contains volcanic and minor sedimentary formations, providing valuable insights into the oldest Svecofennian crust in southern Finland. Previously, felsic volcanic rocks from the Orijärvi, Kisko and Toija formations have been dated at 1895 ± 3, 1878 ± 4 and 1878 ± 4 Ma, respectively. In the present study, the Sorvasto sample from the southern boundary of the Kisko formation yields a zircon age of 1885 ± 5 Ma and a titanite age of 1800 ± 15 Ma. The zircon age falls within the interval between previously obtained age determinations and is coeval with the common Svecofennian crustal growth stage. The Kavasto sample from the western part of the area yields a zircon age of 1878 ± 6 Ma and a titanite age of 1796 ± 4 Ma. The zircon age corresponds to those obtained for similar rock types in the Toija and Ahdisto formations. Picritic interlayers occur within all these successions and are here interpreted as belonging to the same Toija formation. We tentatively infer that the Toija and Salittu formations, together with the overlying sedimentary rocks, can be traced to the West Uusimaa area in the east and the Turku area in the west. The titanite ages near 1.80 Ga reflect cooling or reheating events.

Introduction

Constructing stratigraphic relations in Paleoproterozoic bedrock is difficult, especially in highly deformed terrains such as in southern Finland. Generally, all the supracrustal belts in this region show a complicated internal stratigraphy and structure, since the high metamorphic grade and deformation have largely obliterated the primary structures. The Orijärvi area within the Uusimaa belt is one of the few locations in southernmost Finland (Fig. 1) where metamorphism took place in temperatures below anatexis, in contrast to the surroundings, where migmatites are common. The Orijärvi triangle (Ploegsma and Westra 1990) has escaped major deformation processes, being enveloped by two major shear zones, the Kisko and Jyly shear zones, which led to deformation partitioning into the low strain (Orijärvi) and high strain (West Uusimaa) domains (Skyttä et al. 2006; Fig. 2). These features make the Orijärvi area a suitable location for absolute age determinations in southern Finland and for studying the oldest Svecofennian stratigraphy and tectonism. The combined findings can be used to model a wider tectonic evolution of southern Finland.

Isotopic age determinations on volcanic rocks are scarce in southern Finland but the age of volcanism in the Orijärvi area is reasonably well known. However, because of the complexity of a volcanic arc, internal within-arc age variations are less well-known. In this study, we dated zircons and titanites from two felsic rocks in Orijärvi with the aim to fill the existing gaps that hamper the interpretation of stratigraphy and regional correlation of geological units. All the rock types are metamorphic. Therefore, the prefix 'meta-' is omitted.

Geological setting

The Svecofennian orogen was formed between 1.95 and 1.75 Ga (e.g. Lahtinen et al. 2005). It forms the Proterozoic basement in Finland, parts of Sweden and Norway, and the Lake Ladoga area in northwestern Russia (Gaál and Gorbatschev 1987; Fig. 1A). To the south and southeast, the basement is covered by Paleozoic sedimentary rocks (Soesoo et al. 2020). In the major Svecofennian Province in Finland,

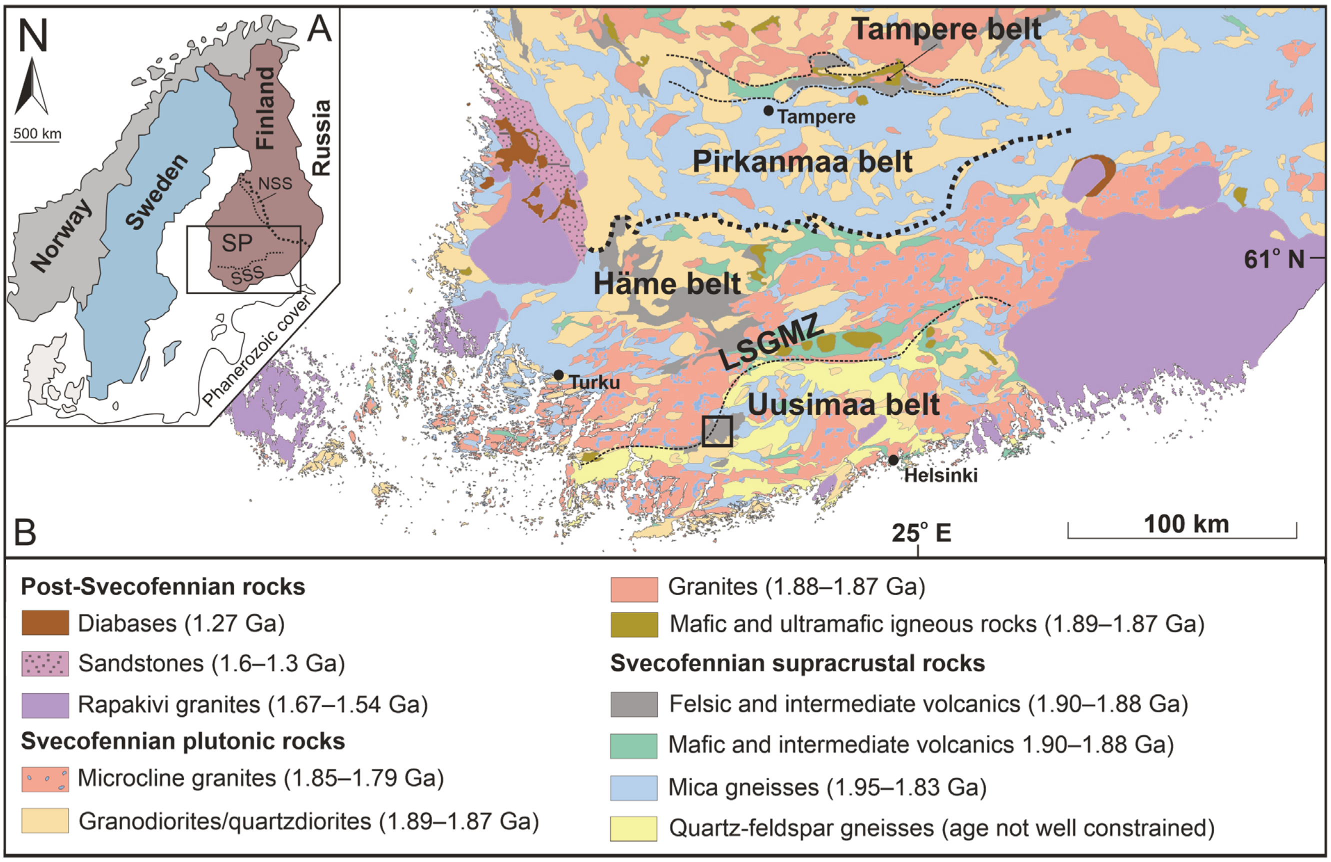

Fig. 1. Location of the study area: **A** – Svecofennian crustal provinces in Finland, **B** – location of the Orijärvi area (black square) on a general geological map of southern Finland, modified from the Bedrock of Finland – DigiKP. The nomenclature follows Nironen (2017a) and Kohonen et al. (2021). Abbreviations: SP – Svecofennian Province, NSS – Northern Svecofennia Subprovince, SSS – Southern Svecofennia Subprovince, LSGMZ – late Svecofennian granite-migmatite zone (Ehlers et al. 1993).

two subprovinces can be distinguished: the Northern and Southern Svecofennia Subprovinces (Kohonen et al. 2021; Fig. 1), which were amalgamated during early Svecofennian tectonism (Lahtinen et al. 2005). The Southern Svecofennia Subprovince is further divided into the Häme and Uusimaa volcano-sedimentary belts (Nironen 2017a).

The Orijärvi area within the Uusimaa belt is a non-migmatised, lower metamorphic grade area within the high grade anatectic late Svecofennian granite-migmatite zone of southern Finland (LSGMZ in Fig. 1; Ehlers et al. 1993). The Orijärvi area contains volcaniclastic and other sedimentary rocks with well-preserved primary structures that were metamorphosed in the andalusite–cordierite stability field (Eskola 1914; Ploegsma and Westra 1990; Skyttä et al. 2006). The area comprises four defined lithostratigraphic formations (Fig. 2): the lowermost Orijärvi formation (fm), Kisko fm, Toija fm and the uppermost Salittu fm (Väisänen and Mänttäri 2002). According to the interpretation of the authors, the Orijärvi and Kisko formations represent growth of the volcanic arc, whereas the Toija and Salittu formations are related to the subsequent rifting stage. This model, based on field relations and the chemostratigraphy of volcanic rocks, has not been fully verified by absolute age determinations. The lithostratigraphic subdivision (Väisänen and Mänttäri 2002) was modified by Nironen et al. (2016) with the addition of two new formations, the Ahdisto and Vetio formations.

Zircons from rhyolite in the Orijärvi fm (low in the stratigraphic sequence) and the Kisko dacite (high in the stratigraphic sequence) were dated using the thermal ionization mass spectrometer (TIMS) at 1895.3 ± 2.4 Ma (later referred to as 1895 ± 3 Ma) and 1878.2 ± 3.4 Ma (later referred to as 1878 ± 4 Ma), respectively (Väisänen and Mänttäri 2002). Zircons from rhyolite in the Toija fm yielded a secondary-ion mass spectrometry (SIMS) age of 1878 ± 4 Ma (Väisänen and Kirkland 2008). In addition, zircons from the synvolcanic Orijärvi granodiorite are dated at 1891 ± 13 Ma (TIMS; Huhma 1986), 1898 ± 9 Ma (SIMS; Väisänen et al. 2002) and 1892 ± 4 Ma (laser ablation mass spectrometer (LAMS); Kara et al. 2018). Within 2 sigma errors, these ages are similar to the age of the Orijärvi rhyolite sample (Fig. 2).

Sampling sites and samples

Two felsic rock samples were collected for uranium–lead (U–Pb) isotope analysis. The Sorvasto sample from the southern boundary of the Kisko fm was collected from a road cut along the Finnish Route Number 186 near Sorvastonlammi. This outcrop is part of felsic volcanics extending in the east–west direction for about 8 km across the whole Orijärvi triangular area between the Kisko and the Jyly shear zones (Fig. 2). In the same rock suite, approximately 500 metres east of Sorvasto, a visibly similar rock type was previously geochemically identified as rhyolite (sample 87.3MV95 in Väisänen and Mänttäri 2002). The outcrop sampled for this study consists of a coarsely layered rock with thick homogeneous tuff layers alternating with volcanic breccia

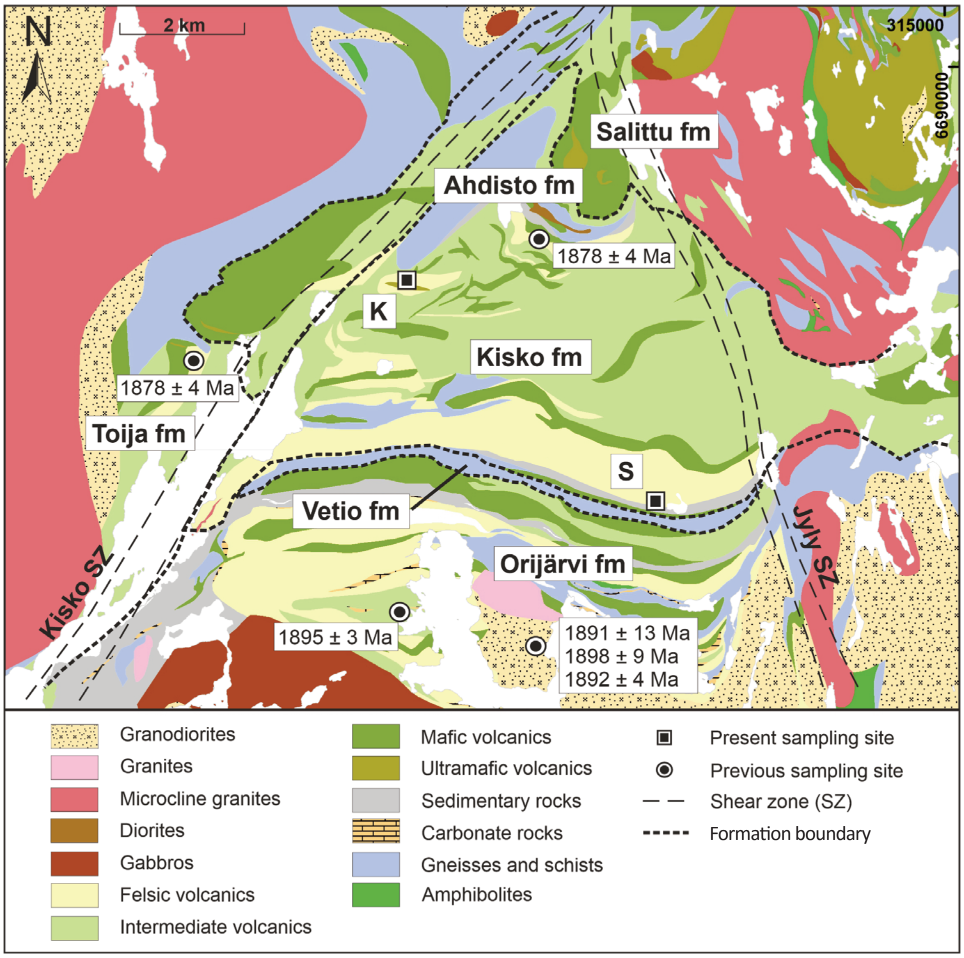

Fig. 2. Geological map of the Orijärvi area, showing the previously suggested formation boundaries (Väisänen and Mänttäri 2002; Nironen et al. 2016), the locations of the published zircon age determinations and the sampling sites of the present study. The map is modified from the Bedrock of Finland – DigiKP, Skyttä et al. (2006) and Kara et al. (2018). Abbreviations: K – Kavasto, S – Sorvasto, fm – formation.

layers. The breccia contains 1–20 cm fragments, whose composition is evidently similar to that in the matrix, only somewhat finer-grained. The sample was taken from a homogeneous layer (Fig. 3A).

Based on thin section examination, the Sorvasto sample is fine- and even-grained, with an average grain size of 0.1 mm. These grains are predominantly anhedral to subhedral. There are a few larger subhedral fragments ranging in size from 0.5 to 2 mm. The main minerals are quartz, plagioclase (oligoclase), K-feldspar and biotite. K-feldspar and plagioclase occur in approximately equal amounts. The larger fragments are predominantly quartz. Variations in mica content impart layering to the rock (Fig. 4A and B). Small feldspar grains are difficult to distinguish under the optical microscope. Therefore, thin sections were also analysed and imaged with scanning electron microscope (SEM) (Fig. 5A).

The Kavasto sample was collected from the northwestern part of the study area, from within the formally defined Kisko fm (Fig. 2). In this area, several rock types occur: mafic and intermediate volcanic rocks, pelitic sedimentary rocks, plagioclase porphyrites (samples KII-30 and KII-31 in Väisänen and Mänttäri 2002) and felsic rocks. The previously analysed 1878 ± 4 Ma dacite (sample 20MV96 in Väisänen and Mänttäri 2002) occurs about 2 km east–northeast of the present locality. Approximately 200 m south of the sampled outcrop is an occurrence of a relatively rare rock type: layered fragment-bearing picrite (Fig. 3C; sample 272MV95 in Väisänen and Mänttäri 2002). Contacts with other rock types are not exposed. The present sampled outcrop is a layered felsic rock with alternating 5–20 cm light-coloured layers and darker, thinner, more fine-grained layers. The sample was taken from a lighter layer (Fig. 3B).

Based on examination of the thin section, the Kavasto sample is extremely fine-grained, with a grain size of around 0.01 mm (Fig. 4C and D). It is relatively even-grained, with grain morphologies mostly subhedral to anhedral. The main minerals are quartz, plagioclase (oligoclase) and biotite. Plagioclase and quartz are present in roughly equal proportions, with micaceous bands defining the banding. Optical mineral identification was verified with SEM mineral analyses and images (Fig. 5B). In the field, the rock was interpreted as a felsic volcanic or volcaniclastic rock but for further discussion, see section ‘Older zircons in the samples’.

Analytical methods

The separation of the zircons and titanites was performed with conventional methods of crushing, grinding, panning and removal of magnetite with a hand magnet. After the heavy liquid (methylene iodide) and Franz magnetic separator runs, the grains were hand-picked, cast in an epoxy mount and polished.

The backscattered electron (BSE) imaging of the zircons and titanites was carried out with two instruments. The Sorvasto sample was imaged using an Apreo S microscope by Thermo Fisher Scientific Inc. at the Department of Physics and Astronomy, University of Turku. The Kavasto sample was imaged with a desktop scanning electron microscope Phenom XL by Thermo Fisher Scientific Inc. at Åbo Akademi

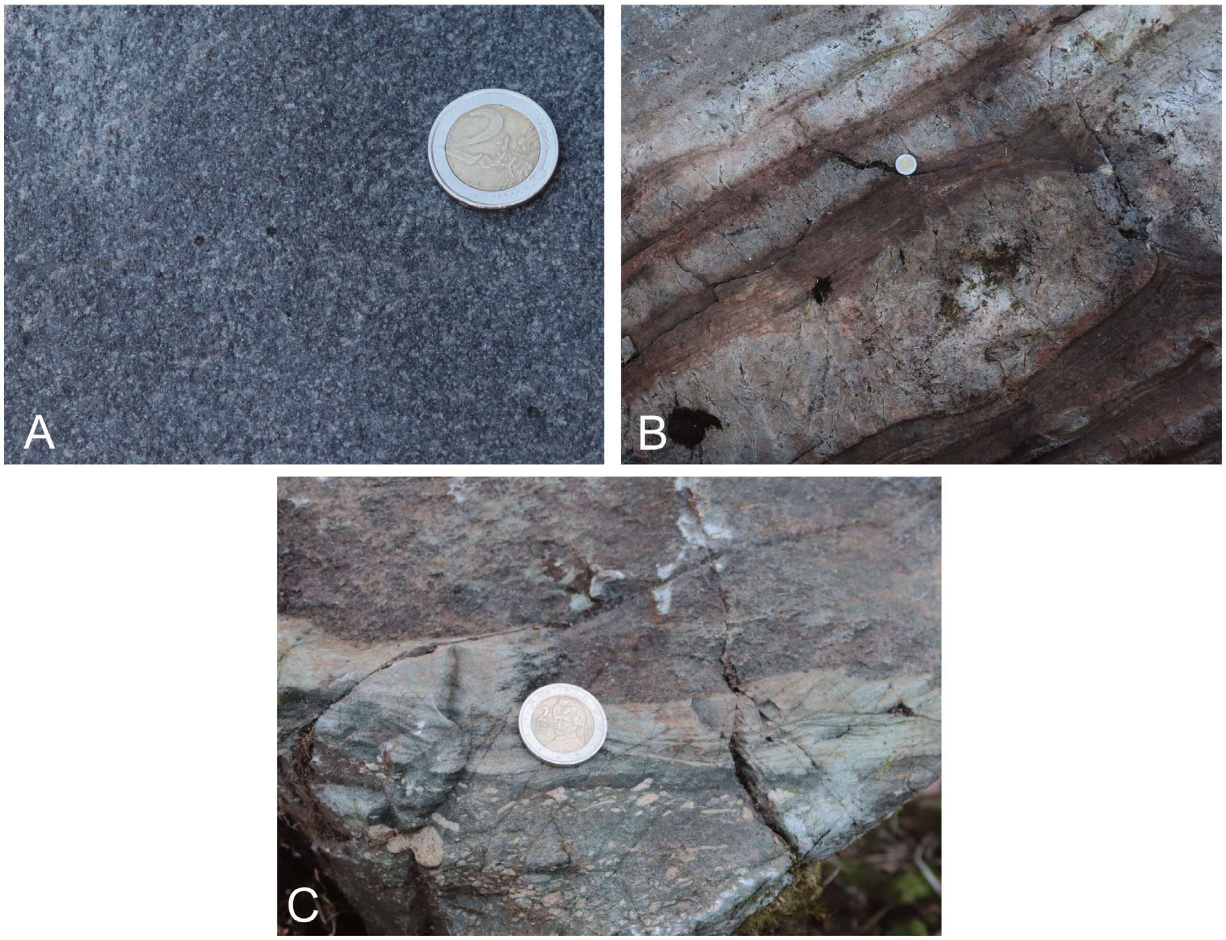

Fig. 3. Field photos of the sampled rocks and a picrite: **A** – Sorvasto, **B** – Kavasto, **C** – layered picrite with small felsic fragments nearby the Kavasto sampling site.

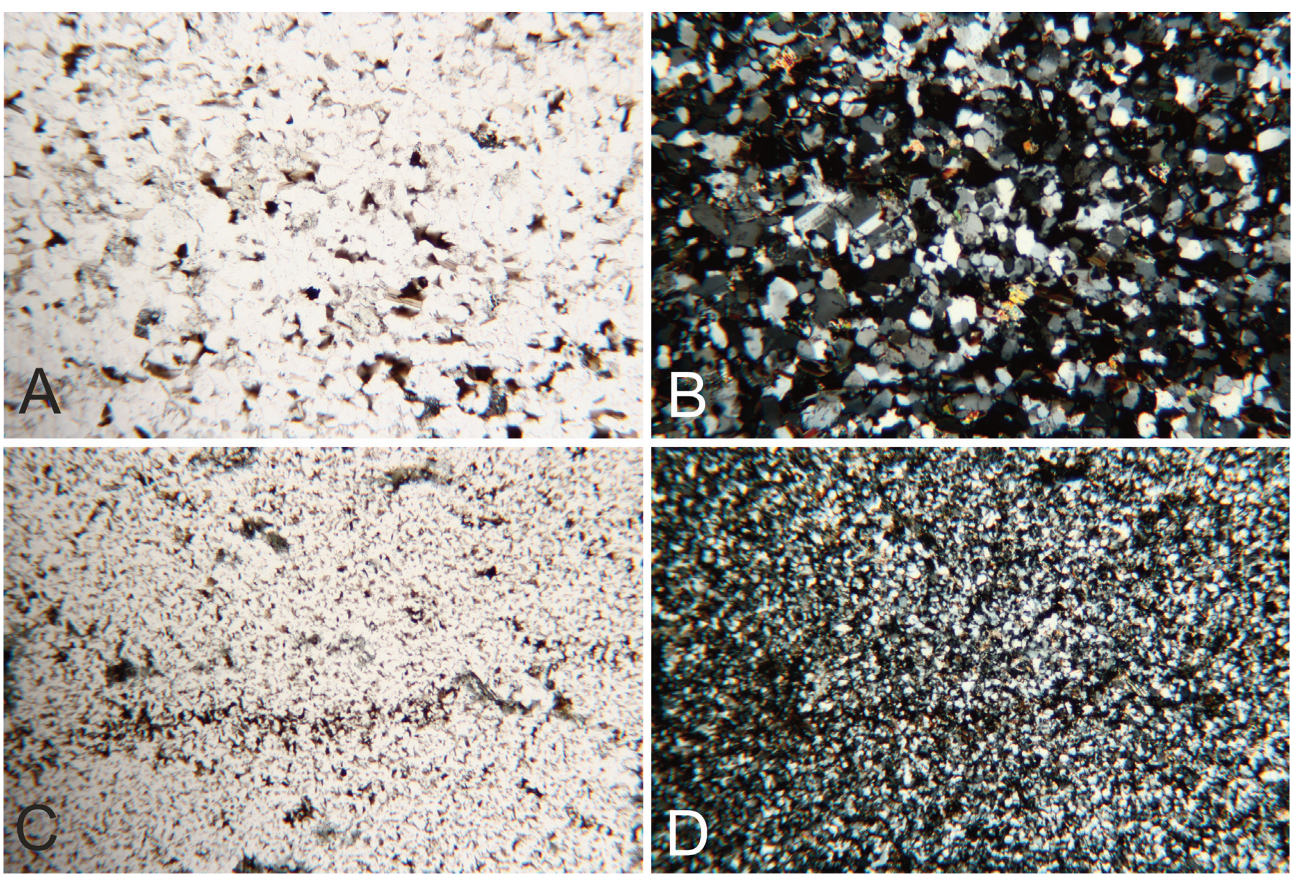

Fig. 4. Thin section photomicrographs of the samples: **A** – Sorvasto, plane-polarised, **B** – Sorvasto, cross-polarised, **C** – Kavasto, plane-polarised, **D** – Kavasto, cross-polarised light. Width of the images is 3 mm.

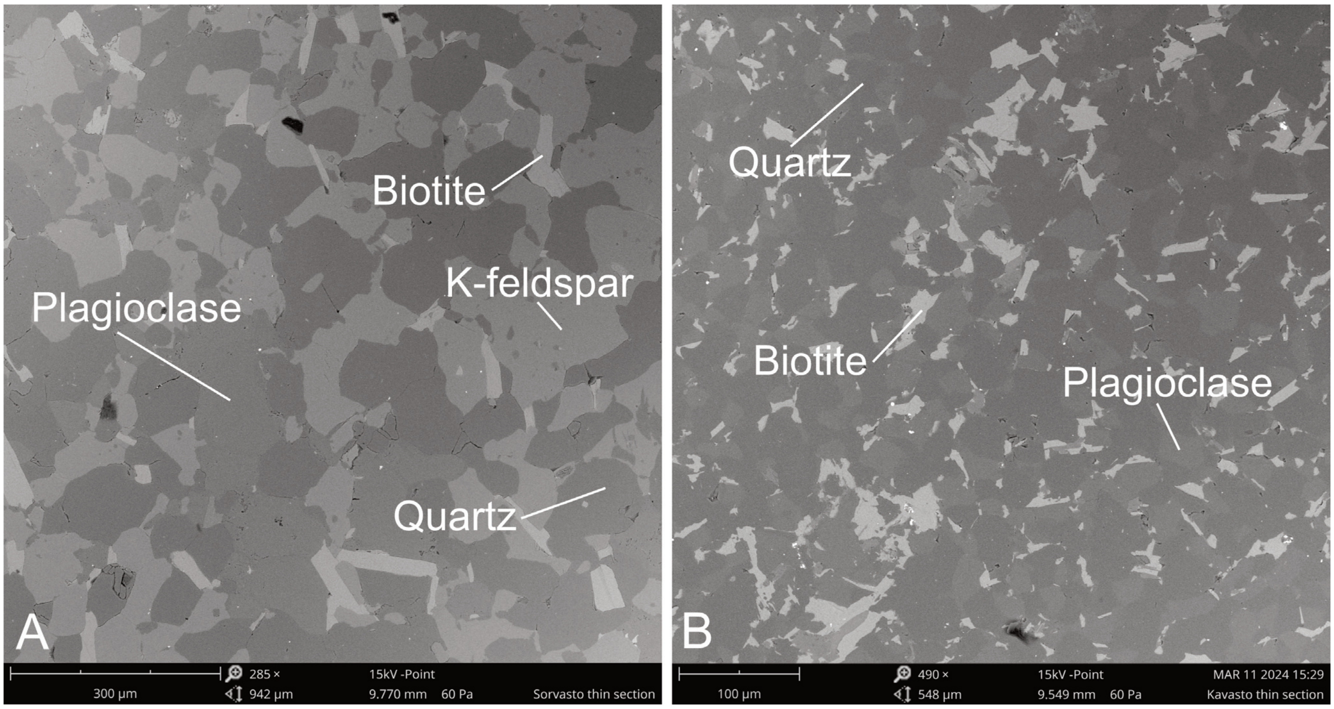

Fig. 5. Backscattered electron images of the samples: **A** – Sorvasto, **B** – Kavasto. Minerals were identified with energy-dispersive X-ray spectroscopy (EDS) analyses.

University, Geohouse, Turku. Thin sections were imaged and minerals were analysed with the same instrument.

The zircon U–Pb isotope age determinations were conducted at the Finnish Geosciences Research Laboratory (SGL) facilities, Geological Survey of Finland, Espoo. The analyses were performed using a Nu Plasma AttoM laser ablation–single collector–inductively coupled plasma–mass spectrometer (LA–SC–ICPMS). Ablation was performed with a Teledyne Excite laser ablation system that was connected to the AttoM device. During analysis, samples were ablated in He gas (gas flow = 0.4 and 0.1 l/min) in a HelEx ablation cell (Müller et al. 2009). Argon was mixed into He aerosol before entering to plasma (Ar gas flow = 0.95 l/min). The laser spot size was 25 µm in diameter and pulse frequency 5 Hz. The energy of the laser was 50% of 5.0 mJ, producing an on-sample fluence of 1.25 J/cm².

Pre-ablation consisted of 10 pulses using a 35 µm spot, followed by 20 seconds with the laser off to sweep clean the cell prior to on-mass background measurement. Ablation for analysis then followed with a 30 second stationary beam. ^{235}U was calculated from the counts measured at mass number ^{238}U, using the natural ratio of $^{238}U/^{235}U$=137.88. The raw data from the analyses were corrected for the background, mass discrimination, laser-induced elemental fractionation and drift in ion counter gains, and reduced to U–Pb isotope ratios by using concordant calibration standard zircons with known ages: GJ-01 (609 ± 1 Ma; Belousova et al. 2006), A382 (1877 ± 2 Ma; Huhma et al. 2012) and A1772 (2712 ± 1 Ma; Huhma et al. 2012). The standards were run at the beginning and end of each sample, as well as during the analytical sessions at roughly regular intervals between every ten sample analyses.

The data reduction for the zircon U–Pb raw data was performed with Glitter 4.4.4 software (Achterberg et al. 2001), which includes visualisation of isotope data and allows the user to calibrate standards and optimise the selection of each analysis based on signal and time. Outliers in the raw data were filtered with Glitter. Further data reduction included error propagation and common Pb corrections, which were calculated with an in-house (SGL) Microsoft Excel spreadsheet written by Yann Lahaye and Hugh O'Brien.

The titanites were analysed at the SGL facilities, using the same equipment and workflow as for the zircons. The diameter of laser spots was 40 µm, with 50 µm pre-ablation with a pulse frequency of 5 Hz. For the Kavasto sample, the laser energy was 45% of 5.0 mJ and fluence 1.40 J/cm². Argon gas flow was 0.94 l/min. For the Sorvasto sample, the laser energy was 35% of 5.0 mJ and fluence 2.54 J/cm². Two known titanite calibration standards were used for quality control during both analytical sessions: MKED-1 (Spandler et al. 2016) and an in-house sample A1756 (1857 Ma, unpublished). The standards were run at the beginning and end for each sample, as well as during analytical sessions at roughly regular intervals between every ten analyses.

The same data reduction procedure was used for the titanite U–Pb raw data as for the zircons. However, the common Pb correction was slightly modified to avoid over-correction of the data. Age calculations and plotting of the final U–Pb isotopic data were carried out using the Isoplot/Ex4.15 program (Ludwig 2012).

Results

Zircon data

Sorvasto sample

The zircons in the Sorvasto sample range from prismatic to subhedral grains, with average lengths of 80–100 µm. The grain colour varies from transparent to light brown. The BSE

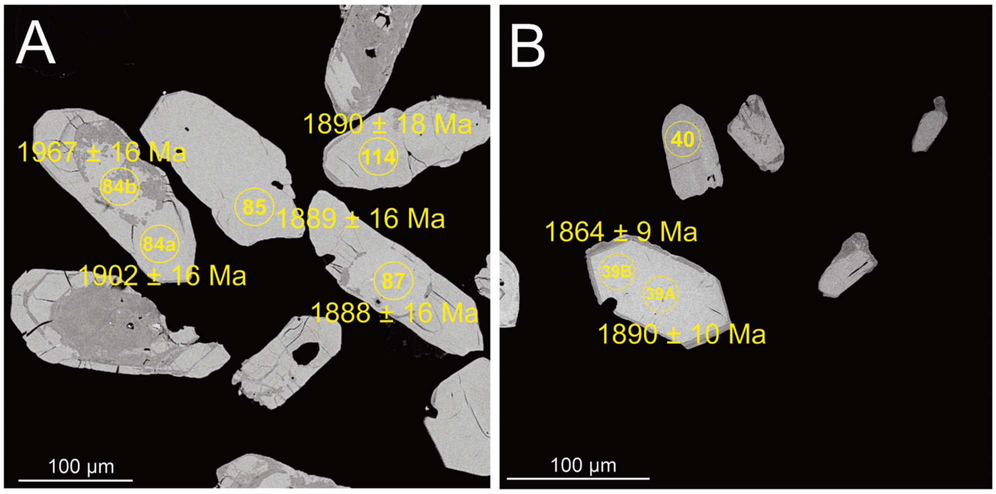

Fig. 6. Backscattered electron images of the representative zircon morphologies: **A** – Sorvasto sample, **B** – Kavasto sample. Yellow circles represent U–Pb analysis spots (25 µm) with their corresponding $^{207}Pb/^{206}Pb$ ages. Numbers and letters within the circles represent sample codes found in Tables 1 and 2.

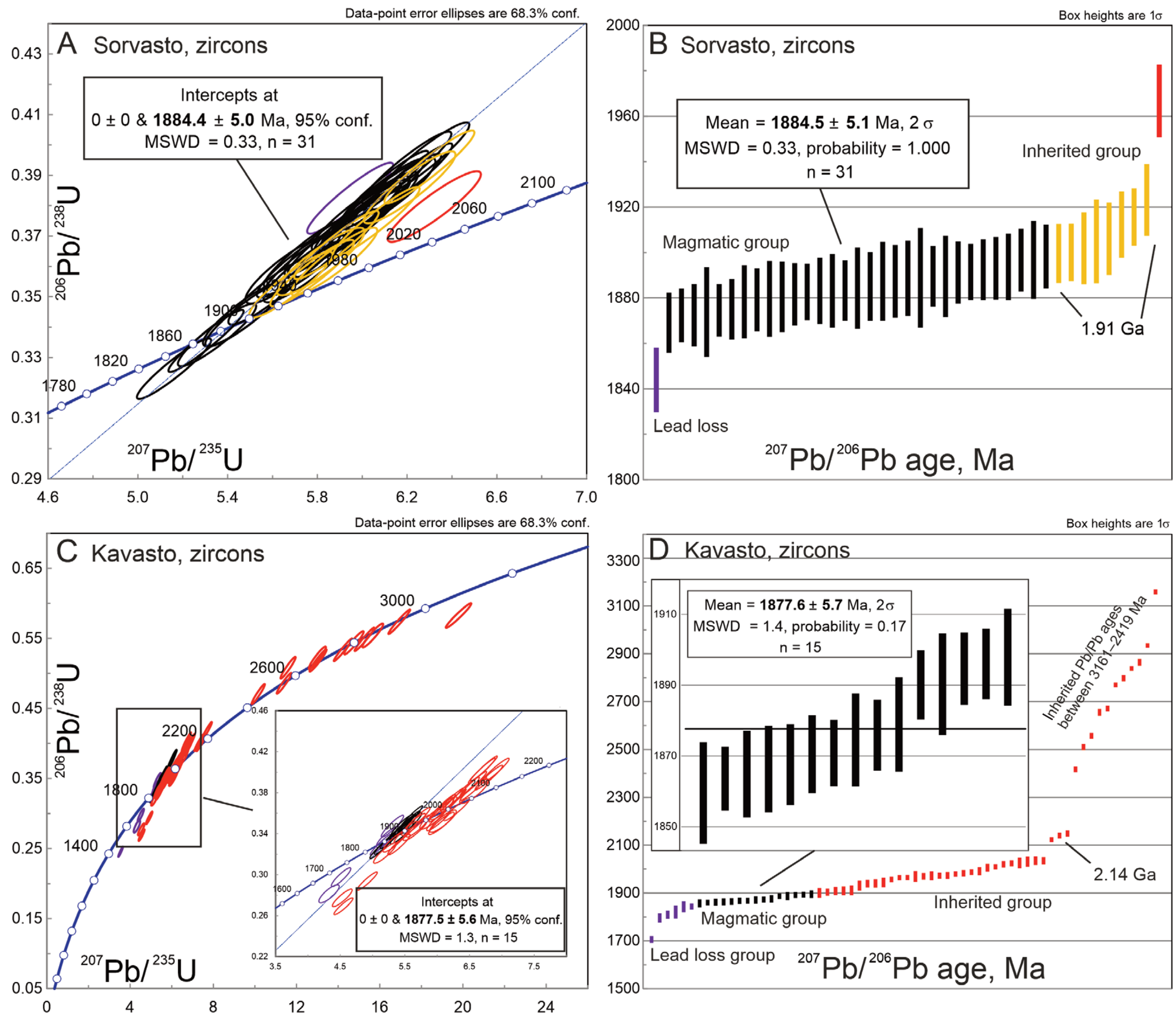

Fig. 7. U–Pb concordia and $^{207}Pb/^{206}Pb$ weighted average age diagrams for the analysed zircons: **A, B** – Sorvasto sample, **C, D** – Kavasto sample. Different colours represent different age populations. Abbreviation: MSWD – mean square weighted deviation.

image (Fig. 6A) shows that many of the grains are fractured. Faint oscillatory zoning and core domains are apparent (Fig. 6A, grain 87). Most of the grains are slightly metamict.

A total of 43 analyses were performed on 38 zircons (Table 1). Two analyses were rejected because of high discordance and high common Pb. Nine analyses resulted in $^{207}Pb/^{206}Pb$ ages ≥1900 Ma and are interpreted as recording inheritance. One of the analyses shows a younger age, likely due to lead loss, and was therefore omitted from the calculations (cf. Corfu 2013). The rest of the analyses form an elongated cluster upon and above the concordia line, yielding an upper intercept age of 1884.4 ± 5.0 Ma (95% conf., MSWD = 0.33; Fig. 7A). The age is similar to the $^{207}Pb/^{206}Pb$ weighted average age of 1884.5 ± 5.1 Ma (2σ, MSWD = 0.33; Fig. 7B), which we prefer. This age is hereinafter referred to as 1885 ± 5 Ma and interpreted as the crystallisation age, which represents an eruptive event.

Table 1. Zircon U–Pb data for the Sorvasto sample

Sample	$^{206}Pb/^{204}Pb$	^{206}Pbc, %	ppm			Ratios						r	Concordance, %	Ages					
			Pb	Th	U	$^{207}Pb/^{206}Pb$	1σ	$^{207}Pb/^{235}U$	1σ	$^{206}Pb/^{238}U$	1σ			$^{207}Pb/^{206}Pb$	1σ	$^{207}Pb/^{235}U$	1σ	$^{206}Pb/^{238}U$	1σ
SR97	6151	0.2799	176	79	412	0.11275	0.00087	5.94639	0.12674	0.38249	0.00772	0.932	113	1844	14	1968	18	2088	36
SR41	455074	0.0038	116	19	295	0.11433	0.00082	5.74492	0.12133	0.36443	0.00736	0.940	107	1869	13	1938	18	2003	35
SR37	11309	0.1522	299	266	656	0.11454	0.00074	6.10071	0.12747	0.38631	0.00778	0.951	112	1873	12	1990	18	2106	36
SR61	7616	0.2260	225	123	502	0.11455	0.00085	6.19838	0.13147	0.39246	0.00792	0.937	114	1873	13	2004	18	2134	37
SR113	165479	0.0104	44	31	109	0.11464	0.00124	5.67223	0.12769	0.35887	0.00732	0.877	105	1874	19	1927	19	1977	35
SR29	1390720	0.0012	376	267	979	0.11468	0.00072	5.30400	0.11059	0.33544	0.00675	0.954	99	1875	11	1870	18	1865	33
SR101	1700167	0.0010	457	312	1240	0.11471	0.00083	5.16091	0.10923	0.32630	0.00658	0.939	97	1875	13	1846	18	1820	32
SR96b	209566	0.0082	56	33	138	0.11492	0.00101	5.71721	0.12393	0.36081	0.00732	0.914	106	1879	16	1934	19	1986	35
SR68	970275	0.0018	274	285	594	0.11498	0.00087	6.08336	0.12931	0.38373	0.00774	0.934	111	1880	14	1988	18	2094	36
SR78	703458	0.0024	200	207	441	0.11500	0.00105	5.97208	0.13022	0.37663	0.00762	0.908	110	1880	16	1972	19	2061	36
SR111	515185	0.0033	139	111	361	0.11506	0.00098	5.35297	0.11538	0.33743	0.00682	0.920	100	1881	15	1877	18	1874	33
SR48a	558284	0.0031	147	66	333	0.11513	0.00086	6.27587	0.13319	0.39536	0.00798	0.936	114	1882	13	2015	18	2148	37
SR6	519891	0.0033	140	108	334	0.11520	0.00078	5.85424	0.12293	0.36858	0.00743	0.947	107	1883	12	1954	18	2023	35
SR96a	381239	0.0045	104	81	249	0.11523	0.00092	5.74727	0.12283	0.36175	0.00731	0.928	106	1883	14	1939	18	1990	35
SR5b	157520	0.0109	42	29	106	0.11523	0.00102	5.58717	0.12118	0.35166	0.00714	0.913	103	1884	16	1914	19	1943	34
SR43	548247	0.0031	149	110	344	0.11524	0.00084	5.97837	0.12635	0.37626	0.00759	0.939	109	1884	13	1973	18	2059	35
SR16	3349	0.5139	129	148	316	0.11530	0.00113	5.47341	0.12090	0.34428	0.00700	0.896	101	1885	18	1896	19	1907	33
SR102	436589	0.0039	120	97	272	0.11535	0.00096	6.01495	0.12924	0.37819	0.00765	0.923	110	1885	15	1978	19	2068	36
SR90	338051	0.0051	92	70	221	0.11549	0.00110	5.75158	0.12622	0.36118	0.00732	0.901	105	1888	17	1939	19	1988	35
SR87	3522118	0.0005	1037	1376	2434	0.11550	0.00101	5.48077	0.11873	0.34417	0.00695	0.914	101	1888	16	1898	18	1907	33
SR85	563334	0.0031	153	116	349	0.11558	0.00105	6.04847	0.13179	0.37955	0.00768	0.909	110	1889	16	1983	19	2074	36
SR117	92937	0.0185	25	21	60	0.11560	0.00140	5.85902	0.13522	0.36760	0.00754	0.853	107	1889	22	1955	20	2018	35
SR42	437059	0.0039	118	84	274	0.11563	0.00084	6.01361	0.12721	0.37719	0.00762	0.939	109	1890	13	1978	18	2063	36
SR114	261466	0.0066	70	41	160	0.11563	0.00114	6.12161	0.13513	0.38396	0.00780	0.896	111	1890	18	1993	19	2095	36
SR47	515329	0.0033	138	86	322	0.11575	0.00086	6.02054	0.12770	0.37725	0.00762	0.936	109	1892	13	1979	18	2063	36
SR19	1226	1.4040	168	160	342	0.11576	0.00078	6.20409	0.13022	0.38869	0.00784	0.947	112	1892	12	2005	18	2117	36
SR48b	692926	0.0025	183	88	424	0.11582	0.00085	6.15422	0.13022	0.38537	0.00777	0.939	111	1893	13	1998	18	2101	36
SR105	802331	0.0021	216	144	507	0.11586	0.00087	5.99003	0.12726	0.37495	0.00756	0.935	108	1893	13	1974	18	2053	35
SR103	561654	0.0031	153	117	355	0.11591	0.00093	5.97577	0.12782	0.37392	0.00755	0.927	108	1894	14	1972	18	2048	35
SR39	344776	0.0050	92	57	218	0.11609	0.00087	5.98046	0.12701	0.37361	0.00755	0.935	108	1897	13	1973	18	2046	35

Continued on the next page

Table 1. *Continued*

Sample	$^{206}Pb/^{204}Pb$	$^{206}Pb_c$, %	ppm			Ratios						r	Concordance, %	Ages					
			Pb	Th	U	$^{207}Pb/^{206}Pb$	1σ	$^{207}Pb/^{235}U$	1σ	$^{206}Pb/^{238}U$	1σ			$^{207}Pb/^{206}Pb$	1σ	$^{207}Pb/^{235}U$	1σ	$^{206}Pb/^{238}U$	1σ
SR108	208365	0.0083	58	54	137	0.11610	0.00110	5.75077	0.12606	0.35924	0.00729	0.902	104	1897	17	1939	19	1979	34
SR21	286763	0.0060	79	66	184	0.11620	0.00089	5.89022	0.12536	0.36765	0.00744	0.933	106	1899	14	1960	18	2018	35
SR30	453901	0.0038	122	82	292	0.11628	0.00083	5.88523	0.12415	0.36707	0.00741	0.942	106	1900	13	1959	18	2016	35
SR8	499405	0.0034	135	85	300	0.11632	0.00080	6.29936	0.13251	0.39279	0.00792	0.945	112	1900	12	2018	18	2136	37
SR84a	1266016	0.0014	354	330	842	0.11643	0.00101	5.68220	0.12310	0.35396	0.00715	0.916	103	1902	16	1929	19	1953	34
SR88	205132	0.0084	56	45	134	0.11663	0.00119	5.81492	0.12910	0.36160	0.00735	0.889	104	1905	18	1949	19	1990	35
SR106	559174	0.0031	160	176	345	0.11670	0.00102	6.21182	0.13471	0.38606	0.00781	0.915	110	1906	16	2006	19	2105	36
SR50	368657	0.0047	100	79	243	0.11711	0.00094	5.77704	0.12357	0.35779	0.00723	0.927	103	1913	14	1943	18	1972	34
SR40	595541	0.0029	161	108	375	0.11733	0.00081	6.06280	0.12756	0.37477	0.00756	0.945	107	1916	12	1985	18	2052	35
SR5a	177631	0.0097	48	36	117	0.11782	0.00102	5.87504	0.12701	0.36165	0.00734	0.916	103	1923	16	1958	19	1990	35
SR84b	280	6.1545	123	51	241	0.12072	0.00107	6.32083	0.13712	0.37974	0.00769	0.913	105	1967	16	2021	19	2075	36
Rejected																			
~~SR63~~	~~390~~	~~4.4163~~	~~392~~	~~177~~	~~570~~	~~0.11761~~	~~0.00083~~	~~8.26271~~	~~0.17427~~	~~0.50955~~	~~0.01027~~	~~0.942~~	~~138~~	~~1920~~	~~13~~	~~2260~~	~~19~~	~~2655~~	~~44~~
~~SR59~~	~~52~~	~~33.0288~~	~~537~~	~~69~~	~~240~~	~~0.20843~~	~~0.00149~~	~~22.56753~~	~~0.47657~~	~~0.78529~~	~~0.01585~~	~~0.941~~	~~129~~	~~2893~~	~~12~~	~~3208~~	~~20~~	~~3736~~	~~57~~

Kavasto sample

The morphology of the zircon grains from Kavasto varies from a few prismatic grains to anhedral and rounded grains, with lengths ranging greatly between 40 and 120 µm. Many grains show faint oscillatory zoning as well as core domains. The grains are occasionally fractured and/or metamict, but less than in the Sorvasto sample zircons (Fig. 6B).

A total of 65 analyses were performed on 52 grains in two sessions (Table 2). One analysis was rejected due to disturbance during the analysis and high discordance. Multiple age populations can be identified from the dataset. Forty-two analyses resulted in $^{207}Pb/^{206}Pb$ ages between 2937 and 1904 Ma (Fig. 7C and D). Many of these ages originate from the middle parts of zircon grains, which occasionally display separate core areas. Some of the older ages in turn originate from the edges of zircon grains. Some grains also display similar old ages from the middle of the grain. We interpret these zircons as inherited.

The upper intercept age of the main group of 15 analyses is 1877.5 ± 5.6 Ma (95% conf., MSWD = 1.3; Fig. 7C). This group yields a similar $^{207}Pb/^{206}Pb$ weighted average age of 1877.6 ± 5.7 Ma (2σ, MSWD = 1.4; Fig. 7D). These are hereinafter referred to as 1878 ± 6 Ma. The six youngest ages are interpreted to have suffered lead loss and were omitted from calculations (cf. Corfu 2013).

Titanite data

Sorvasto sample

The titanite grains in the Sorvasto sample have rough edges, and some grains are broken. The grains are euhedral in shape, and some are slightly elongated, 100–250 µm in size (Fig. 8A).

A total of eight spots on eight grains were analysed (Table 3). The analyses are concordant but one of them shows an about 30 Ma younger age, presumably due to lead loss. The seven analyses form a cluster, which yields a concordia age of 1802 ± 13 Ma (2σ, MSWD = 0.33; Fig. 9A). The $^{207}Pb/^{206}Pb$ weighted average age for the same analyses is 1800 ± 15 Ma (2σ, MSWD = 0.19; Fig. 9B).

Kavasto sample

The titanite grains in the Kavasto sample are mostly light brown and larger than the zircon grains, varying in size from 100 to 200 µm. The shapes vary from euhedral to rounded and broken. All grain types were selected for U–Pb analyses. The BSE images of the selected grains are shown in Fig. 8B.

A total of 30 analyses were performed on 28 titanite grains (Table 4). One analysis was rejected due to high common Pb value and discordancy. Two of the analyses are clearly older at about 1.84 Ga, while four grains form a cluster with a $^{207}Pb/^{206}Pb$ weighted average age of about 1.82 Ga. The main group of 22 analyses yields a concordia age of 1796 ± 4.1 Ma (2σ, MSWD = 5.6; Fig. 9C) and a similar $^{207}Pb/^{206}Pb$ weighted average age of 1795.6 ± 4.1 Ma (2σ, MSWD = 0.32; Fig. 9D). These are hereafter referred to as 1796 ± 4 Ma. The youngest grain has apparently suffered from lead loss and was omitted from calculations.

Table 2. Zircon U–Pb data for the Kavasto sample

Sample	$^{206}Pb/^{204}Pb$	^{206}Pbc, %	ppm			Ratios						ρ	Concordance, %	Ages					
			Pb	Th	U	$^{207}Pb/^{206}Pb$	1σ	$^{207}Pb/^{235}U$	1σ	$^{206}Pb/^{238}U$	1σ			$^{207}Pb/^{206}Pb$	1σ	$^{207}Pb/^{235}U$	1σ	$^{206}Pb/^{238}U$	1σ
KR-14	1767	0.9742	125	73	453	0.10469	0.00067	3.54059	0.07439	0.24529	0.00495	0.953	83	1709	12	1536	17	1414	26
KR-25a	10336	0.1666	191	164	568	0.10998	0.00104	4.51229	0.09949	0.29757	0.00604	0.904	93	1799	17	1733	18	1679	30
4B	3804	0.4526	99	61	260	0.11083	0.00090	5.30799	0.11367	0.34736	0.00701	0.926	106	1813	15	1870	18	1922	33
KR-19	2488	0.6918	60	71	184	0.11151	0.00154	4.32661	0.10381	0.28139	0.00583	0.820	88	1824	25	1698	20	1598	29
KR-25b	670372	0.0026	169	158	442	0.11283	0.00131	5.24149	0.12027	0.33692	0.00688	0.864	101	1845	21	1859	19	1872	33
4A	10555	0.1631	181	137	496	0.11290	0.00066	5.12497	0.10609	0.32923	0.00662	0.960	99	1847	11	1840	17	1835	32
KR-27	1498	1.1492	53	85	125	0.11372	0.00090	5.46077	0.11726	0.34828	0.00706	0.930	104	1860	14	1894	18	1926	34
39B	4487	0.3836	90	120	209	0.11397	0.00057	5.60039	0.11475	0.35638	0.00716	0.970	105	1864	9	1916	18	1965	34
KR-38	3214	0.5356	123	107	325	0.11406	0.00077	5.12258	0.10819	0.32574	0.00657	0.948	97	1865	12	1840	18	1818	32
13	401	4.2974	110	148	252	0.11414	0.00077	5.19336	0.10879	0.32998	0.00665	0.947	98	1866	12	1852	18	1838	32
KR-8	304298	0.0057	76	86	200	0.11423	0.00072	5.28587	0.11088	0.33562	0.00677	0.954	100	1868	11	1867	18	1866	33
27	5891	0.2922	86	132	213	0.11441	0.00069	5.43482	0.11286	0.34452	0.00693	0.957	102	1871	11	1890	18	1908	33
38	8280	0.2079	143	135	361	0.11443	0.00059	5.44978	0.11192	0.34541	0.00694	0.968	102	1871	9	1893	17	1913	33
KR-39c	9018	0.1909	175	313	391	0.11467	0.00083	5.50483	0.11706	0.34819	0.00703	0.940	103	1875	13	1901	18	1926	34
2B	1701706	0.0010	309	398	750	0.11475	0.00063	5.56139	0.11472	0.35150	0.00706	0.964	104	1876	10	1910	18	1942	34
1	5973	0.2882	44	51	110	0.11494	0.00085	5.49592	0.11616	0.34678	0.00700	0.938	102	1879	13	1900	18	1919	33
39A	656050	0.0026	125	195	265	0.11566	0.00062	6.05020	0.12457	0.37939	0.00763	0.965	110	1890	10	1983	18	2073	36
8	359794	0.0048	63	53	161	0.11567	0.00092	5.57966	0.11909	0.34985	0.00707	0.929	102	1890	14	1913	18	1934	34
2A	12865	0.1338	220	227	501	0.11595	0.00065	5.97340	0.12340	0.37362	0.00751	0.962	108	1895	10	1972	18	2046	35
36A	10216	0.1685	129	89	320	0.11604	0.00064	5.72995	0.11811	0.35812	0.00720	0.964	104	1896	10	1936	18	1973	34
KR-36b	505191	0.0034	125	89	327	0.11616	0.00088	5.45157	0.11652	0.34037	0.00688	0.935	99	1898	14	1893	18	1888	33
KR-32	21227	0.0811	283	24	805	0.11654	0.00119	5.34166	0.11960	0.33244	0.00675	0.889	97	1904	18	1876	19	1850	33
KR-1	164304	0.0105	42	43	101	0.11672	0.00078	5.70769	0.12031	0.35467	0.00717	0.949	103	1907	12	1933	18	1957	34
7	288787	0.0060	53	77	132	0.11707	0.00095	5.51175	0.11798	0.34145	0.00690	0.926	99	1912	14	1902	18	1894	33
22	4163	0.4135	37	83	84	0.11710	0.00103	5.63457	0.12185	0.34897	0.00708	0.914	101	1912	16	1921	18	1930	34
KR-20	6661	0.2585	233	100	665	0.11724	0.00116	5.19064	0.11554	0.32109	0.00653	0.896	94	1915	18	1851	19	1795	32
KR-33	314844	0.0055	86	150	251	0.11852	0.00119	4.53201	0.10102	0.27734	0.00564	0.893	82	1934	18	1737	18	1578	28
16	6399	0.2690	145	191	382	0.11908	0.00090	5.40843	0.11469	0.32941	0.00664	0.935	94	1942	13	1886	18	1836	32
40	8888	0.1937	72	98	180	0.11912	0.00099	5.70664	0.12258	0.34744	0.00704	0.922	99	1943	15	1932	18	1922	34
12	1529570	0.0011	256	73	692	0.11940	0.00118	5.66125	0.12479	0.34388	0.00696	0.894	98	1947	18	1925	19	1905	33

Continued on the next page

Table 2. *Continued*

Sample	$^{206}Pb/^{204}Pb$	^{206}Pbc, %	ppm			Ratios						ρ	Concordance, %	Ages					
			Pb	Th	U	$^{207}Pb/^{206}Pb$	1σ	$^{207}Pb/^{235}U$	1σ	$^{206}Pb/^{238}U$	1σ			$^{207}Pb/^{206}Pb$	1σ	$^{207}Pb/^{235}U$	1σ	$^{206}Pb/^{238}U$	1σ
42B	8003	0.2151	80	131	174	0.12024	0.00060	6.09230	0.12480	0.36748	0.00738	0.970	103	1960	9	1989	18	2018	35
41A	44052	0.0391	477	233	1071	0.12077	0.00057	6.72113	0.13733	0.40364	0.00810	0.973	111	1968	8	2075	18	2186	37
42A	11220	0.1534	85	67	185	0.12081	0.00059	6.68859	0.13695	0.40155	0.00807	0.971	111	1968	9	2071	18	2176	37
KR-30b	9183	0.1875	114	139	275	0.12113	0.00137	5.93548	0.13564	0.35540	0.00726	0.869	99	1973	20	1966	20	1960	34
11	9129	0.1886	158	32	390	0.12113	0.00077	6.24411	0.13034	0.37388	0.00752	0.952	104	1973	11	2011	18	2048	35
KR-30a	8927	0.1928	163	195	385	0.12129	0.00112	6.10241	0.13399	0.36489	0.00740	0.907	102	1975	16	1991	19	2005	35
37	5194	0.3314	42	54	97	0.12131	0.00071	6.06224	0.12551	0.36244	0.00730	0.960	101	1976	10	1985	18	1994	34
5B	1915	0.8988	79	67	236	0.12137	0.00085	4.91619	0.10345	0.29378	0.00592	0.943	84	1976	12	1805	18	1660	29
47B	8110	0.2123	75	103	165	0.12179	0.00063	6.25227	0.12845	0.37231	0.00749	0.968	103	1983	9	2012	18	2040	35
47A	358635	0.0048	66	74	146	0.12197	0.00075	6.44877	0.13391	0.38345	0.00773	0.956	105	1985	11	2039	18	2092	36
41B	68516	0.0251	520	578	1156	0.12237	0.00063	6.56097	0.13472	0.38887	0.00781	0.968	106	1991	9	2054	18	2118	36
26	12353	0.1394	186	208	594	0.12257	0.00097	4.54966	0.09702	0.26921	0.00543	0.928	77	1994	14	1740	18	1537	28
15	2716	0.6339	49	42	122	0.12358	0.00097	6.03055	0.12839	0.35391	0.00716	0.930	97	2009	14	1980	18	1953	34
21A	13012	0.1323	170	198	371	0.12389	0.00061	6.56058	0.13440	0.38407	0.00771	0.971	104	2013	9	2054	18	2095	36
21B	12243	0.1406	198	275	410	0.12457	0.00077	6.89516	0.14341	0.40143	0.00808	0.955	108	2023	11	2098	18	2176	37
35	4101	0.4198	106	106	232	0.12489	0.00073	6.79984	0.14067	0.39488	0.00795	0.960	106	2027	10	2086	18	2145	37
18	179	9.6391	20	17	35	0.12498	0.00140	6.57209	0.14836	0.38137	0.00790	0.869	103	2029	20	2056	20	2083	37
6	757473	0.0023	140	184	335	0.12536	0.00132	6.08868	0.13629	0.35225	0.00716	0.883	96	2034	18	1989	19	1945	34
17	1252	1.3752	30	24	73	0.12566	0.00109	6.06449	0.13088	0.35004	0.00711	0.916	95	2038	15	1985	19	1935	34
KR-5	4570	0.3767	71	43	172	0.12566	0.00088	6.30341	0.13355	0.36382	0.00736	0.944	98	2038	12	2019	18	2000	35
45	921028	0.0019	158	69	353	0.13209	0.00057	7.30817	0.14874	0.40128	0.00805	0.977	102	2126	8	2150	18	2175	37
31A	9128	0.1886	144	99	299	0.13338	0.00072	7.68804	0.15831	0.41804	0.00840	0.965	105	2143	9	2195	18	2252	38
31B	14332	0.1201	206	154	452	0.13405	0.00076	7.41307	0.15319	0.40106	0.00806	0.961	101	2152	10	2163	18	2174	37
10	2983	0.5770	132	134	222	0.15658	0.00087	10.15844	0.20971	0.47053	0.00946	0.963	103	2419	9	2449	19	2486	41
44A	3260	0.5280	27	26	42	0.16548	0.00100	11.59452	0.24060	0.50816	0.01027	0.957	105	2512	10	2572	19	2649	44
44B	175515	0.0098	35	44	56	0.17021	0.00097	11.40076	0.23562	0.48579	0.00980	0.961	100	2560	10	2556	19	2552	42
24	331921	0.0052	66	68	99	0.18050	0.00126	12.99809	0.27339	0.52227	0.01056	0.943	102	2657	12	2680	20	2709	45
23	19783	0.0870	348	11	602	0.18230	0.00103	13.03172	0.26920	0.51845	0.01042	0.962	101	2674	9	2682	19	2693	44
43A	1361247	0.0013	281	367	397	0.19347	0.00090	14.23487	0.29083	0.53362	0.01072	0.974	99	2772	8	2765	19	2757	45
29	9556	0.1801	84	46	129	0.19685	0.00133	14.75718	0.30930	0.54371	0.01098	0.947	100	2800	11	2800	20	2799	46

Continued on the next page

Table 2. *Continued*

Sample	$^{206}Pb/^{204}Pb$	^{206}Pbc, %	ppm			Ratios						ρ	Concordance, %	Ages					
			Pb	Th	U	$^{207}Pb/^{206}Pb$	1σ	$^{207}Pb/^{235}U$	1σ	$^{206}Pb/^{238}U$	1σ			$^{207}Pb/^{206}Pb$	1σ	$^{207}Pb/^{235}U$	1σ	$^{206}Pb/^{238}U$	1σ
43B	1117572	0.0015	235	301	317	0.20182	0.00095	15.26452	0.31197	0.54855	0.01102	0.973	99	2841	8	2832	19	2819	46
46B	5678	0.3032	71	33	105	0.20502	0.00148	15.66707	0.33046	0.55422	0.01124	0.940	99	2867	12	2857	20	2843	46
46A	483790	0.0036	94	54	130	0.21412	0.00094	16.93856	0.34509	0.57375	0.01153	0.977	100	2937	7	2931	19	2923	47
34	25312	0.0680	376	212	515	0.24629	0.00125	19.78530	0.40600	0.58262	0.01170	0.969	94	3161	8	3081	20	2959	47
Rejected																			
~~5A~~	~~6844~~	~~0.2515~~	~~142~~	~~93~~	~~708~~	~~0.11487~~	~~0.00091~~	~~2.94504~~	~~0.06291~~	~~0.18594~~	~~0.00375~~	~~0.928~~	~~59~~	~~1878~~	~~14~~	~~1394~~	~~16~~	~~1099~~	~~20~~

Table 3. Titanite U–Pb data for the Sorvasto sample

Sample	$^{206}Pb/^{204}Pb$	ppm			Ratios						ρ	Concordance, %	Ages					
		Pb	Th	U	$^{207}Pb/^{206}Pb$	1σ	$^{207}Pb/^{235}U$	1σ	$^{206}Pb/^{238}U$	1σ			$^{207}Pb/^{206}Pb$	1σ	$^{207}Pb/^{235}U$	1σ	$^{206}Pb/^{238}U$	1σ
Kisko-SC21C-5ttn	1877	47	11	178	0.10779	0.00116	4.61366	0.14611	0.31043	0.00984	0.942	99	1762	20	1752	26	1743	48
Kisko-SC21C-2ttn	2033	38	16	135	0.10947	0.00118	4.88072	0.15462	0.32336	0.01025	0.942	101	1791	20	1799	26	1806	50
Kisko-SC21C-4ttn	2410	45	43	153	0.10974	0.00118	4.93146	0.15611	0.32591	0.01033	0.942	101	1795	19	1808	26	1819	50
Kisko-SC21C-3bttn	2013	43	36	152	0.10977	0.00121	4.79178	0.15202	0.31661	0.01004	0.940	99	1796	20	1783	26	1773	49
Kisko-SC21C-1ttn	1314	36	35	123	0.10989	0.00118	4.88397	0.15462	0.32233	0.01022	0.942	100	1798	19	1799	26	1801	50
Kisko-SC21C-7ttn	1307	38	12	133	0.11012	0.00119	4.96865	0.15742	0.32723	0.01038	0.942	101	1801	20	1814	26	1825	50
Kisko-SC21C-3attn	2102	40	27	138	0.11013	0.00118	4.97966	0.15766	0.32793	0.01040	0.942	101	1802	19	1816	26	1828	50
Kisko-SC21C-6ttn	1424	24	28	79	0.11108	0.00121	5.05134	0.16009	0.32980	0.01046	0.941	101	1817	20	1828	27	1837	51

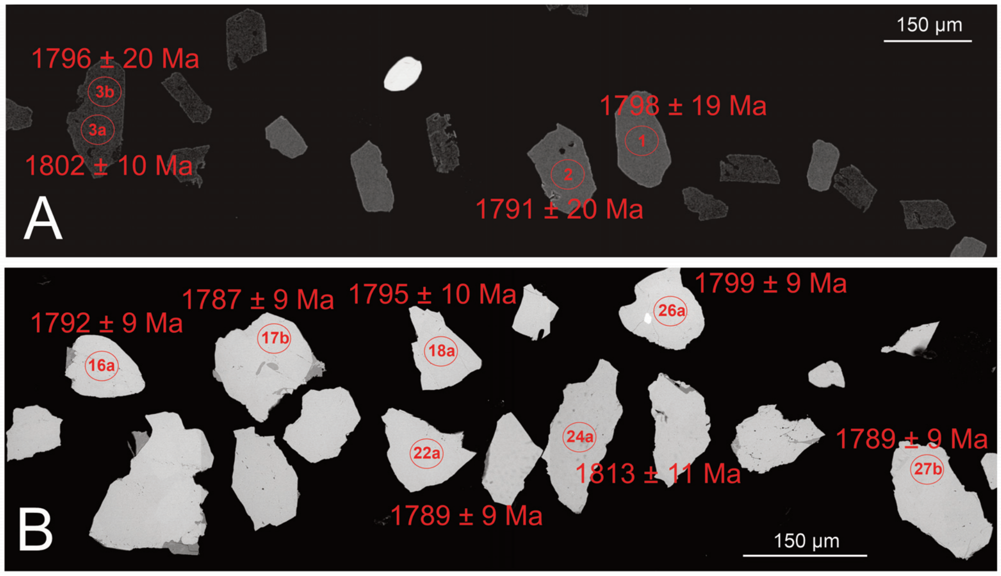

Fig. 8. Backscattered electron images of the representative titanite morphologies: **A** – Sorvasto sample, **B** – Kavasto sample. Red circles represent U–Pb analysis spots (40 µm) with their corresponding $^{207}Pb/^{206}Pb$ ages. Numbers and letters within the circles represent sample codes found in Tables 3 and 4.

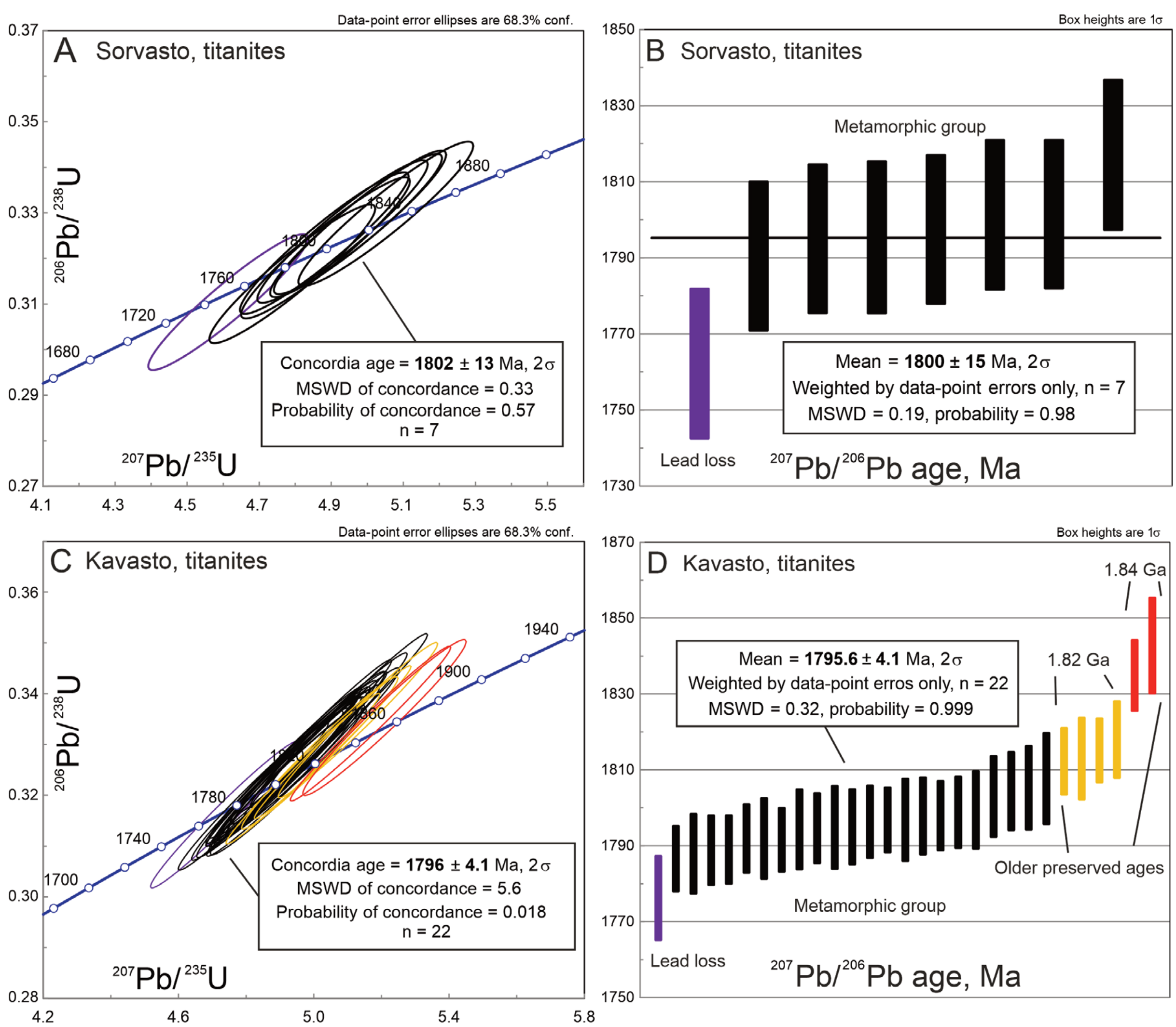

Fig. 9. U–Pb concordia and $^{207}Pb/^{206}Pb$ weighted average age diagrams for the titanites: **A**, **B** –Sorvasto sample, **C**, **D** – Kavasto sample. Different colours represent different age populations.

Table 4. Titanite U–Pb data for the Kavasto sample

Sample	$^{206}Pb/^{204}Pb$	ppm			Ratios						ρ	Concordance, %	Ages					
		Pb	Th	U	$^{207}Pb/^{206}Pb$	1σ	$^{207}Pb/^{235}U$	1σ	$^{206}Pb/^{238}U$	1σ			$^{207}Pb/^{206}Pb$	1σ	$^{207}Pb/^{235}U$	1σ	$^{206}Pb/^{238}U$	1σ
KRT-58a	840	35	37	115	0.10862	0.00066	4.73561	0.14416	0.31620	0.00953	0.980	100	1776	11	1774	25	1771	47
KRT-17b	1848	43	11	159	0.10924	0.00051	4.91652	0.14870	0.32641	0.00983	0.988	102	1787	9	1805	25	1821	48
KRT-38a	892	30	27	102	0.10932	0.00063	4.82149	0.14653	0.31988	0.00964	0.982	100	1788	10	1789	25	1789	47
KRT-22a	2362	38	8	140	0.10938	0.00055	4.90615	0.14857	0.32532	0.00980	0.986	101	1789	9	1803	25	1816	47
KRT-27b	2044	46	8	165	0.10939	0.00054	5.00090	0.15138	0.33158	0.00999	0.987	103	1789	9	1819	25	1846	48
KRT-16a	971	34	25	119	0.10956	0.00054	4.90720	0.14854	0.32484	0.00979	0.987	101	1792	9	1803	25	1813	47
KRT-60a	1657	37	9	134	0.10956	0.00064	4.86273	0.14784	0.32190	0.00970	0.982	100	1792	11	1796	25	1799	47
KRT-7a	1857	47	19	175	0.10954	0.00050	4.90502	0.14825	0.32476	0.00978	0.988	101	1792	8	1803	25	1813	47
KRT-18a	616	19	7	64	0.10970	0.00063	4.98188	0.15144	0.32936	0.00993	0.982	102	1795	10	1816	25	1835	48
KRT-13a	1162	30	5	108	0.10972	0.00055	4.93973	0.14962	0.32651	0.00984	0.986	101	1795	9	1809	25	1821	48
KRT-59a	797	30	5	104	0.10974	0.00066	4.87886	0.14847	0.32245	0.00972	0.980	100	1795	11	1799	25	1802	47
KRT-36a	812	31	26	104	0.10975	0.00059	4.95801	0.15043	0.32765	0.00987	0.984	102	1795	10	1812	25	1827	48
KRT-32b	619	32	11	109	0.10983	0.00057	4.98719	0.15117	0.32934	0.00992	0.985	102	1797	9	1817	25	1835	48
KRT-11a	1162	45	25	159	0.10985	0.00051	4.91638	0.14864	0.32459	0.00977	0.988	101	1797	8	1805	25	1812	47
KRT-42a	826	22	9	77	0.10986	0.00065	4.92905	0.14999	0.32542	0.00981	0.981	101	1797	11	1807	25	1816	48
KRT-10a	591	19	3	65	0.10992	0.00061	5.04436	0.15318	0.33284	0.01003	0.983	103	1798	10	1827	25	1852	48
KRT-31a	2234	46	8	168	0.10992	0.00055	4.93990	0.14955	0.32593	0.00982	0.986	101	1798	9	1809	25	1819	48
KRT-26a	269	30	7	88	0.10998	0.00057	5.10209	0.15459	0.33647	0.01014	0.985	104	1799	9	1836	25	1870	49
KRT-41a	717	24	6	83	0.11002	0.00062	4.92279	0.14953	0.32453	0.00978	0.983	101	1800	10	1806	25	1812	47
KRT-45a	1954	30	5	106	0.11023	0.00064	4.96727	0.15104	0.32683	0.00985	0.981	101	1803	11	1814	25	1823	48
KRT-45b	1558	36	9	130	0.11031	0.00062	4.90913	0.14913	0.32275	0.00973	0.983	100	1805	10	1804	25	1803	47
KRT-37a	414	20	6	64	0.11037	0.00067	5.02195	0.15286	0.33002	0.00995	0.980	102	1805	11	1823	25	1838	48
KRT-40a	467	14	5	47	0.11051	0.00073	4.92239	0.15037	0.32304	0.00975	0.977	100	1808	12	1806	25	1805	47
KRT-4a	1390	35	10	131	0.11079	0.00053	4.96813	0.15030	0.32523	0.00980	0.987	100	1812	9	1814	25	1815	47
KRT-24a	437	17	10	55	0.11083	0.00065	5.01794	0.15265	0.32836	0.00990	0.981	101	1813	11	1822	25	1830	48
KRT-2a	3383	45	7	169	0.11097	0.00051	5.05594	0.15283	0.33045	0.00995	0.988	101	1815	8	1829	25	1841	48
KRT-15a	408	19	4	60	0.11114	0.00062	5.13042	0.15578	0.33479	0.01009	0.983	102	1818	10	1841	25	1862	49
KRT-1	431	25	11	80	0.11218	0.00058	5.16790	0.15659	0.33412	0.01007	0.986	101	1835	9	1847	25	1858	48
KRT-40b	498	12	7	38	0.11267	0.00078	5.20897	0.15945	0.33531	0.01013	0.974	101	1843	13	1854	26	1864	49
Rejected																		
~~KRT-34a~~	~~556~~	~~34~~	~~8~~	~~87~~	~~0.10772~~	~~0.00056~~	~~6.25646~~	~~0.18967~~	~~0.42124~~	~~0.01269~~	~~0.985~~	~~129~~	~~1761~~	~~9~~	~~2012~~	~~26~~	~~2266~~	~~57~~

Discussion

Zircon age data

The present study investigated two new locations for age determinations on felsic volcaniclastic rocks from the Sorvasto and Kavasto sites in the Orijärvi area. The results provide significant clarification and confirmation regarding the local and regional stratigraphic positions of the dated rock units. Some analyses are reversely discordant, which is attributable to the matrix effect, i.e. the difference between the reference material and the unknowns (e.g. Marillo-Sialer et al. 2016). However, this only slightly detracts from the reliability of ages, since we use both the U–Pb and $^{207}Pb/^{206}Pb$ calculations, which are almost identical. We prefer the $^{207}Pb/^{206}Pb$ ages because of lack of U–Pb fractionation effect and lower Pb loss effect compared to the concordia ages.

The Sorvasto sample from the lower part of the Kisko fm yields zircon $^{207}Pb/^{206}Pb$ and U–Pb ages of 1885 ± 5 Ma. The age obtained here is younger than that of the Orijärvi fm (1895 ± 3 Ma) and suggests that the Kisko fm overlies the Orijärvi fm, as assumed in the previous study (Väisänen and Mänttäri 2002).

The Kavasto sample provides more information on the northwestern part of the Orijärvi triangle. The age of 1878 ± 6 Ma is interpreted as the magmatic crystallisation age (see section 'Older zircons in the samples' for further discussion). The obtained age corresponds to the previously dated dacite from the northern part of the Kisko fm (1878 ± 4 Ma; Väisänen and Mänttäri 2002), which was redefined as the Ahdisto fm by Nironen et al. (2016). The rhyolite from the Toija fm also yielded a similar age of 1878 ± 4 Ma (Väisänen and Kirkland 2008). All three formations, which share broadly similar ages, also exhibit many common lithological features, including the spatial association with rare picritic volcanic rocks, which have only been observed at higher stratigraphic levels. Further east, a tonalitic intrusion dated at 1878 ± 5 Ma intrudes the Salittu metabasalts, which are interbedded with picrites. Similar ultramafic volcanics also occur in Kavasto, which indicates that 1878 ± 5 Ma represents a minimum age for the Kavasto sample as well.

Older zircons in the samples

The dated samples contain zircons older than the preferred crystallisation ages. This is especially true for the Kavasto sample, where nearly 75% of the analysed spots are older, while in the Sorvasto sample, about 20% are regarded as inherited. These proportions are probably arbitrary because of biased sampling, separation and selection of analysis spots. In Kavasto, the largest and most transparent grains proved to belong to older populations, while the smaller, slightly metamict grains are younger. Since larger, higher-quality grains were preferentially chosen for analysis, this potentially skewed the ratio of older to younger populations.

The Sorvasto sample contains older grains with $^{207}Pb/^{206}Pb$ ages between 1.92–1.90 Ga. These ages form a slightly reversely discordant cluster with an upper intercept age of 1.91 Ga (Fig. 7), probably originating from a single 1.91 Ga source. Additionally, there is a reversely discordant grain dating to 1.97 Ga.

The Kavasto sample resulted in ages ranging between 3.16 and 1.90 Ga, though these do not form distinctly separate clusters, except for the 2.14 Ga and 1.92–1.90 Ga analyses (Fig. 7). Such a plethora of ages suggests a sedimentary origin for these grains, either (1) through contamination with sediments while in transit to the surface or (2) during deposition by derivation from a source terrain with zircons of this age range. Preservation of inherited zircons is controlled by the temperature of the magma, subdivided into cold and hot magmas. Zircons can survive in cooler magmas but dissolve in hotter ones (Miller et al. 2003). Bea et al. (2007), in their case study on the Cambro–Ordovician rocks from the Central Iberian Zone, examined calc-alkaline granites and metavolcanic rocks from 18 samples and found that 70–95% of zircons were inherited. As the magmas were regarded as having been relatively hot, they concluded that, in addition to the temperature, the rate at which magma generates and ascends also affects the preservation of inherited zircons.

In the present case, option 1 could account for the older grains, which were entrained in the magma ascending through a thick volcanic arc with sediment intercalations. Recently, Salminen and Kurhila (2023) studied detrital zircons from metasedimentary rocks in southern Finland, and the zircon populations resemble those in this study. In a related study, Claesson et al. (1993) analysed detrital zircons from the Svecofennian domain and included an Orijärvi sample from Sorvastonlammi, close to the Sorvasto sample. Their Orijärvi sample contained one 2.74 Ga grain and Proterozoic ages between 2.1 and 1.93 Ga. Although we did not find these age populations in the Sorvasto sample, they are present in the Kavasto sample. If the older zircons were sourced from exposed provenance areas during deposition (option 2), the layered Kavasto rock type is a mixed rock (tuffite), and the older grains are part of the sedimentary portion of the tuffite. Nevertheless, the small amount of biotite and the absence of K-feldspar in the Kavasto thin section suggest a volcanic origin for the sample.

In total, there are three options for interpreting the Kavasto ages. First, the magma may have contained all the older zircons, in addition to the 1878 Ma grains that crystallised from the magma. Second, the rock could represent a tuffite, where the younger grains crystallised from the magma while the older grains resided in the sediment. Third, all the zircons may have derived from an external source area of diverse ages, with 1878 Ma representing the maximum deposition age. Since the maximum deposition and minimum ages would be the same, we consider the igneous origin of the 1878 Ma grains the most likely alternative.

Titanite age data

The titanite ages from both Sorvasto and Kavasto are close to 1.80 Ga. The Kavasto sample also contains two older titanite grains at 1.84 Ga (red in Fig. 9D) and four grains at 1.82 Ga (yellow in Fig. 9D). However, most of the analyses yielded the preferred age of 1.80 Ga. Previously, a titanite sample was collected from the northern part of the Kisko fm, east of the Kavasto sampling site (now the Toija fm). The titanite from a dacitic rock sample yielded a concordant TIMS age of 1798 ± 3 Ma (Väisänen and Mänttäri 2002). They interpreted that this approximately 1.8 Ga age refers to reheating of the crust or cooling through the blocking temperature for titanite. The behaviour of titanite in magmatic and metamorphic systems is well studied but complex, since its closure temperature is dependent on several factors. It can be as high as 700 °C but titanite is highly reactive and its closure temperature varies with pressure and the availability of fluids (Frost et al. 2001). Additionally, titanite commonly has high concentrations of common Pb, which complicates reliable age calculations (Kirkland et al. 2018).

The peak metamorphism in Orijärvi took place at about 600 °C and 3 kbars (Latvalahti 1979; Schumacher and Czank 1987). Therefore, the difference of c. 80 million years between the zircon and titanite ages of the present samples is problematic. We propose that the titanite ages reflect cooling, and the titanite was primarily crystallised directly from magma but was recrystallised during the peak metamorphism (possibly around 1.82 Ga). Subsequently, as temperatures steadily decreased, the titanite isotope system was closed at 1.80 Ga. The 1.84 and 1.82 Ga ages observed in the present study, along with the older 1.85–1.84 Ga ages found by Torvela and Kurhila (2022), can be explained by the ability of titanite to retain an older isotopic signature in some grains or subgrains within individual grains (Kohn 2017). An alternative explanation is that the reheating of the crust at 1.80 Ga led to partial recrystallisation of the titanite, since magmatism of that age is common in southern Finland (e.g. Rutanen et al. 2011). Recrystallisation of zircon at 1795 Ma was also detected within the Jyly Shear Zone (Väisänen and Kirkland 2008).

A similar case is observed in Garpenberg, central Sweden, where volcanic rocks are about 1895 Ma in age, while titanites give ages that are about 40 million years younger, at roughly 1.86 Ga. This younger age is interpreted to reflect the age of metamorphism (Jansson and Allen 2011).

Implications for the timing of volcanism and the superposition of the supracrustal units

Previously, the age relations of the formations in the Orijärvi triangle were poorly constrained, leaving a 17-million-year age gap between the Orijärvi fm and the northern part of the Kisko fm (Väisänen and Mänttäri 2002; Nironen et al. 2016). The present age determination from the Sorvasto sample (1885 Ma) in the lower part of the Kisko fm apparently reduces this gap, allowing for a subdivision of the formations into three consecutive age groups (Figs 10 and 11). No major

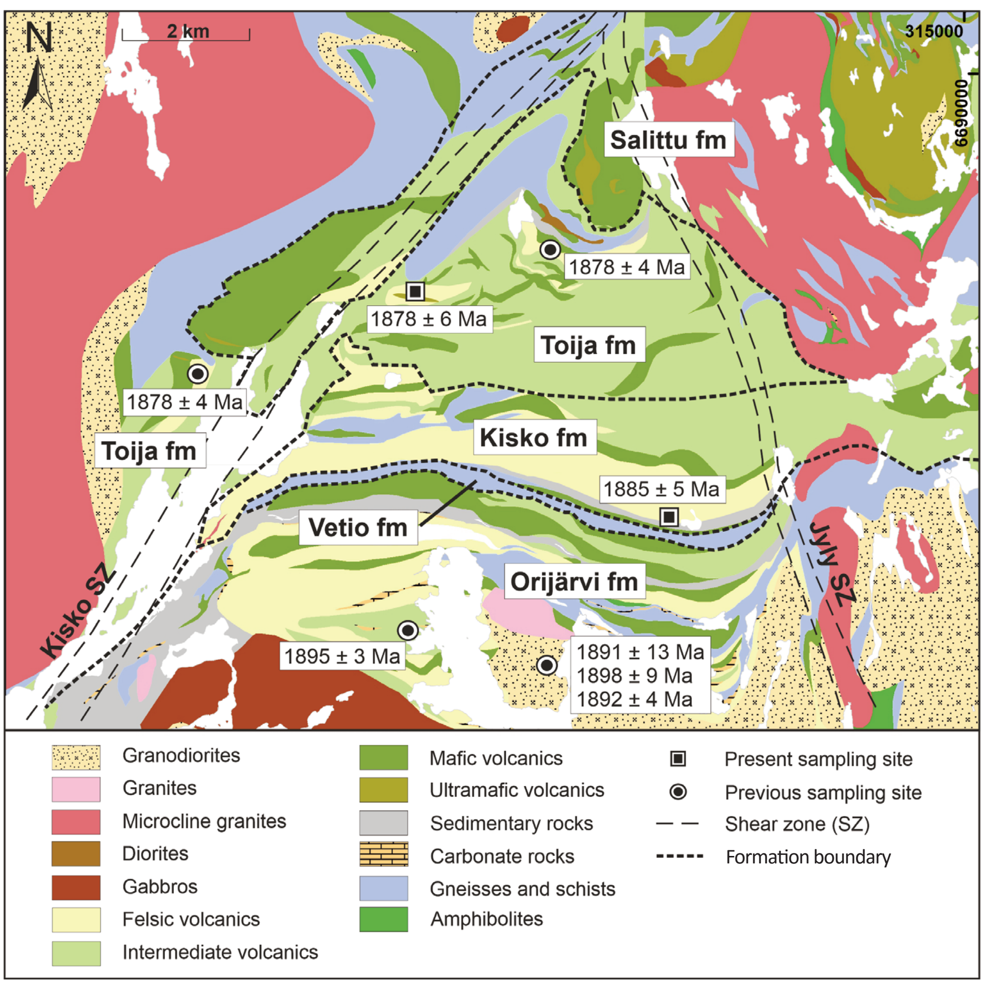

Fig. 10. Revised schematic map of the formation boundaries in the Orijärvi area. The Ahdisto fm has been eliminated, and the Toija fm is extended into the inside of the triangle bounded by Kisko and Jyly shear zones. The new boundary between the Toija and Kisko formations is indicated. Modified from the Bedrock of Finland – DigiKP, Skyttä et al. (2006) and Kara et al. (2018).

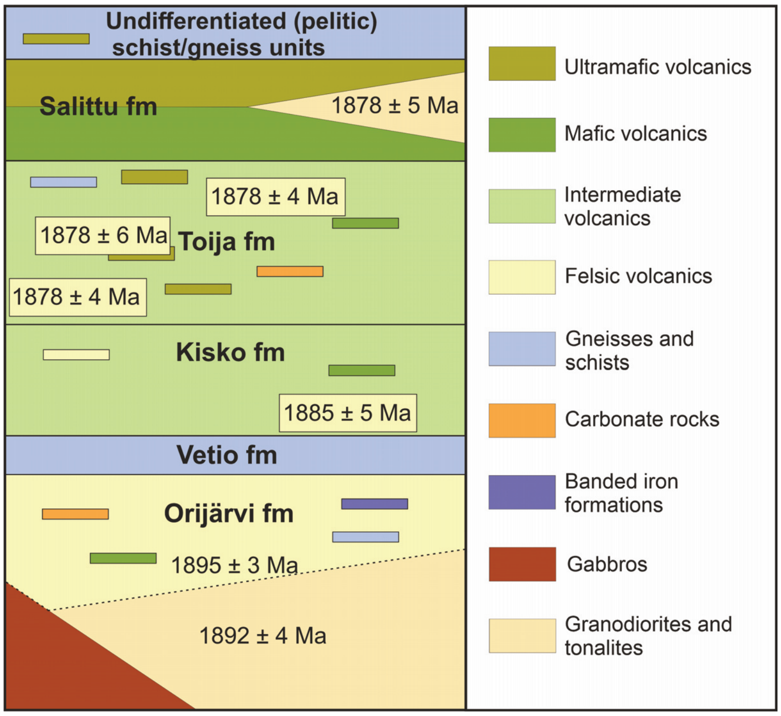

Fig. 11. Lithostratigraphic column of the Orijärvi area, modified from Nironen et al. (2016). Formations are not to scale. Synvolcanic granodiorite is after Colley and Westra (1987), Väisänen and Mänttäri (2002), Nironen et al. (2016) and Kara et al. (2018).

discordances were found in the previous investigations (Väisänen and Mänttäri 2002; Skyttä et al. 2006; Nironen et al. 2016).

The same rock types and ages observed in the Toija and the uppermost Kisko (Ahdisto) formations call into question the justification for assigning them to different formations, when they are situated so closely to one another, even though separated by the Kisko Shear Zone. We propose that all three of these locations are part of the same formation, which we designate here as the Toija fm, as first introduced by Väisänen and Mänttäri (2002). However, the location of the boundary between the Kisko and Toija formations within the Orijärvi triangle remains obscure (Fig. 10). The quartz-feldspar and biotite gneisses located east of the Jyly Shear Zone, below the Salittu fm, are correlated with the Toija fm as defined in this study (formerly the Ahdisto fm, as per Nironen et al. (2016)). This correlation supports the interpretation that the Toija fm is wider than previously interpreted. Thus, the present Toija fm is present both to the west and east of the Kisko Shear Zone and to the east of the Jyly Shear Zone.

The picrites mainly occur at higher stratigraphic levels within the Salittu fm. The ultramafic volcanic rocks can be followed for at least 40 km from Toija village towards the east–northeast, based on information published in the Suomusjärvi and Lohja geological maps as well as positive anomalies in aeromagnetic maps (Salli 1955; Laitala 1994; Nironen et al. 2016).

The Salittu fm (Schreurs et al. 1986; Nironen 2017b) is apparently overlain by a thick sequence of pelitic sedimentary rocks, which now are migmatitic garnet-cordierite mica gneisses (e.g. Schreurs and Westra 1986). Within these sediments, picritic intercalations occur (Salli 1955; field observations by the authors). This strongly suggests that sedimentation and ultramafic volcanism are approximately coeval and belong to the same extensional event.

All the ages combined, Figs 10 and 11 present a revised formation map and lithostratigraphic column of the Orijärvi area, respectively. These representations are derived from available field relations and age determinations. In case of the Salittu fm, the age is inferred from field relations (Väisänen and Mänttäri 2002; Nironen et al. 2016).

Regional correlation

The present data allow to discuss regional stratigraphy and tectonics also outside the Orijärvi area. However, the correlation is only tentative due to significant differences in metamorphic grade and structural evolution (e.g. Ploegsma and Westra 1990).

The lowermost units in the Orijärvi area include the Orijärvi granodiorite, located in the core of a regional upright antiform, and the Orijärvi fm on its northern limb (Figs 10 and 12). On the southern limb of the antiform is the 1891 ± 4 Ma Kuovila felsic tuff, which is coeval with the Orijärvi fm (Skyttä et al. 2005). The antiformal structure, with an east–west fold axis (see Skyttä et al. 2006 for more details), and similar rock types extending both east and west from Orijärvi suggest potential correlation (A in Fig. 12). The rock types at Kemiö are similar: bimodal volcanic rocks, clastic sedimentary rocks and marbles. Moreover, a felsic volcanic rock at Kemiö was dated at 1888 ± 11 Ma (Reinikainen 2001). However, the extent of the Kisko fm outside the Orijärvi area remains unknown.

The extent of the Toija fm is greater than previously inferred. Features typical of the Toija fm, such as bimodal c. 1878 Ma volcanism with transitional mafic rocks of mid-ocean ridge (MORB) affinity and incipient ultramafic volcanism, have been observed throughout the Orijärvi area and probably beyond. This MORB-type volcanism, especially with associated ultramafic variants, is relatively rare in southern Finland, having been found in only a few places

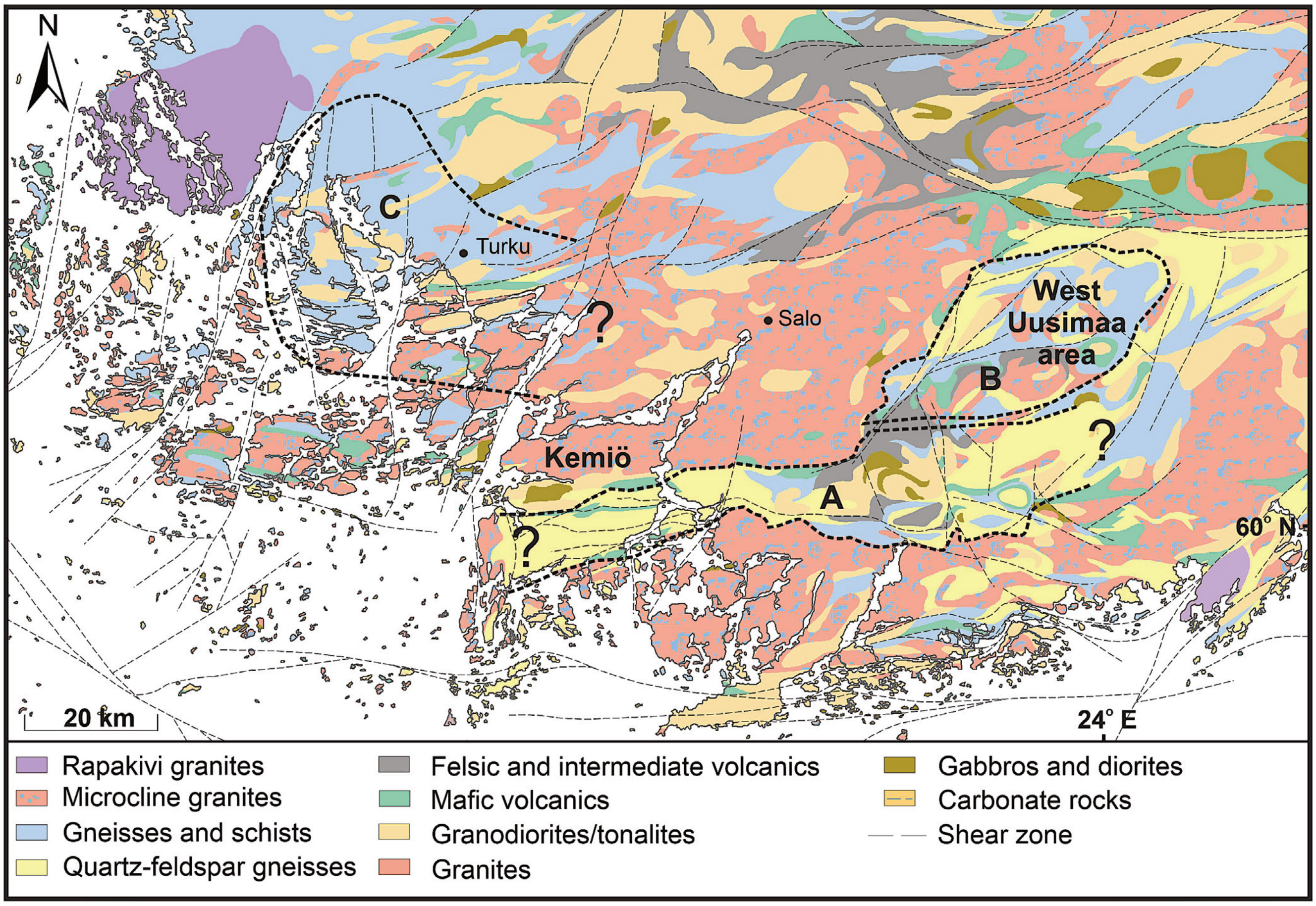

Fig. 12. Orijärvi, Toija and Salittu formations with their possible correlative rock units outside the Orijärvi triangle: **A** – non-migmatitic area west of Orijärvi, **B** – migmatitic area east–northeast of Orijärvi, **C** – migmatitic Turku area in the west. Modified from the Bedrock of Finland – DigiKP.

(Nironen 2017b). These occur in extensional tectonic settings, which probably represent the same event across different regions (cf. Kara et al. 2021). To the east, across the Jyly Shear Zone, the felsic gneisses might correspond to the Toija fm (Ahdisto; Nironen et al. 2016). In the West Uusimaa granulite area (Schreurs and Westra 1986), pelitic migmatites, felsic gneisses, mafic volcanic rocks, picrites and minor marbles dominate the supracrustal rocks. The presence of picrites, which are distinctive due to their rarity, indicates that, at least in the northern part of the West Uusimaa area, these rocks can be correlated with the Toija and Salittu formations (B in Fig. 12). To the west of Orijärvi, the geological continuity is disrupted and obscured by abundant late-orogenic granites and migmatites (e.g. the Perniö granite; Selonen et al. 1996). However, in the Turku area, within the Pargas and Turku groups, mafic volcanic rocks occur among pelitic migmatites, which also possess transitional MORB-type compositions, resembling those of the Toija fm (Väisänen and Mänttäri 2002). Moreover, there are extensive marble deposits in Pargas. The Turku granulite area resembles the West Uusimaa area in terms of protolith and granulite facies metamorphism, and may be coeval, as previously inferred by Väisänen and Westerlund (2007). This tentative regional correlation is shown in Fig. 12.

The Toija and Salittu formations, along with the overlying sediments, were formed during the same tectonic event, namely the 1878 Ma extension. After the arc growth (the Orijärvi and Kisko formations), tectonism switched to extension, initiating basin subsidence. Firstly, bimodal volcanism and carbonate rocks deposited and in the later stage incipient ultramafic volcanism occurred, concomitant with felsic volcanism. As rifting intensified, magmatism progressed entirely to the mantle-derived tholeiitic mafic and ultramafic volcanism of the Salittu fm (cf. Nironen 2017b). Continued extension deepened the basin(s) and led to the simultaneous filling of the basin(s) with erosional sediments, accompanying the waning mantle-derived ultramafic magmatism that manifests as interlayers within the sediments.

The model invoking short-term alternating compressional and extensional episodes during subduction in the Svecofennian orogeny was presented by Hermansson et al. (2008). This model was further utilised by Kara et al. (2020, 2021, 2022), who modelled the enriched MORB (E-MORB)-type and within plate lava (WPL)-type magmatism in the Tampere and Pirkanmaa/Häme belts. Extensional episodes were identified at 1.92–1.90 Ga, 1.89 Ga and 1.86 Ga. In the present study, we introduce the concept of a 1.88 Ga (1878 Ma) extensional stage in southernmost Finland. However, this extensional stage must have been short-lived, since the nearby 1876 ± 4 Ma intermediate mafic dyke intrudes the orogenic deformation (Skyttä et al. 2006).

Conclusions

1. Two U–Pb zircon and two titanite age determinations from the Orijärvi area are presented.
2. The Sorvasto sample from the southern boundary of the Kisko formation is dated at 1885 ± 5 Ma and the Kavasto sample from the western part of the Orijärvi triangle at 1878 ± 6 Ma.
3. The results of the titanite age determinations (c. 1.80 Ga) correspond to the previous results from the Orijärvi area and plausibly reflect lower temperature cooling or reheating during this period.
4. The Kavasto sample is coeval with the previously dated Toija and Ahdisto formations. These formations, all associated with ultramafic volcanic rocks, are now combined and named as the Toija formation.
5. The Toija formation, representing incipient rifting, and the Salittu formation, representing a more intense rifting stage, were formed during the same extensional event. It is proposed that similar rock types formed during the same event throughout the Turku and West Uusimaa areas.

Data availability statement

All the data used here are published in this article.

Acknowledgements

We thank Alvar Soesoo and Peter Sorjonen-Ward for their reviews and comments, which greatly helped to enhance the manuscript. Arto Peltola is thanked for preparing the epoxy mounts and thin sections, and Sören Fröjdö and Ermei Mäkilä for their assistance with SEM imaging and analysis. We also thank Nils Jansson, Ville Järvinen, and Jarmo Kohonen for their advice. This study was partly funded by the K. H. Renlund Foundation to Teemu Vehkamäki and Jaakko Kara. The publication costs of this article were partially covered by the Estonian Academy of Sciences.

References

van Achterberg, E., Ryan, C., Jackson, S. and Griffin, W. 2001. Data reduction software for LA–ICP–MS. In *Laser-Ablation-ICPMS in the Earth Sciences – Principles and Applications* (Sylvester, P., ed.). Mineralogical Association of Canada, St John, Newfoundland, 239–243.

Bea, F., Montero, P., González-Lodeiro, F. and Talavera, C. 2007. Zircon inheritance reveals exceptionally fast crustal magma generation processes in Central Iberia during the Cambro–Ordovician. *Journal of Petrology*, **48**(12), 2327–2339. https://doi.org/10.1093/petrology/egm061

Belousova, E. A., Griffin, W. L. and O'Reilly, S. Y. 2006. Zircon crystal morphology, trace element signatures and Hf isotope composition as a tool for petrogenetic modelling: examples from eastern Australian granitoids. *Journal of Petrology*, **47**(2), 329–353. https://doi.org/10.1093/petrology/egi077

Claesson, S., Huhma, H., Kinny, P. D. and Williams, I. S. 1993. Svecofennian detrital zircon ages – implications for the Precambrian evolution of the Baltic Shield. *Precambrian Research*, **64**(1–4), 109–130. https://doi.org/10.1016/0301-9268(93)90071-9

Colley, H. and Westra, L. 1987. The volcano-tectonic setting and mineralization of the early Proterozoic Kemiö–Orijärvi–Lohja Belt, SW Finland. *Geological Society, London, Special Publication*, **33**(1), 95–107. http://dx.doi.org/10.1144/GSL.SP.1987.033.01.08

Corfu, F. 2013. A century of U–Pb geochronology: the long quest towards concordance. *GSA Bulletin*, **125**(1–2), 33–47. https://doi.org/10.1130/B30698.1

Ehlers, C., Lindroos, A. and Selonen, O. 1993. The late Svecofennian granite-migmatite zone of southern Finland – a belt of transpressive deformation and granite emplacement. *Precambrian Research*, **64**(1–4), 295–309. https://doi.org/10.1016/0301-9268(93)90083-E

Eskola, P. 1914. *On the Petrology of the Orijärvi Region in Southwestern Finland*. Bulletin de la Commission Géologique de Finlande, **40**. Printing-Office of the Imperial Senate, Helsinki.

Frost, B. R., Chamberlain, K. R. and Schumacher, J. C. 2001. Sphene (titanite): phase relations and role as a geochronometer. *Chemical Geology*, **172**(1–2), 131–148. https://doi.org/10.1016/S0009-2541(00)00240-0

Gaál, G. and Gorbatschev, R. 1987. An outline of the Precambrian evolution of the Baltic Shield. *Precambrian Research*, **35**, 15–52. https://doi.org/10.1016/0301-9268(87)90044-1

GTK (Geological Survey of Finland). *Bedrock of Finland – DigiKP. Digital map database, v. 2.1.* Geological Survey of Finland, Espoo. https://gtkdata.gtk.fi/Kalliopera/index.html (accessed 2023-06-01).

Hermansson, T., Stephens, M. B., Corfu, F., Page, L. M. and Andersson, J. 2008. Migratory tectonic switching, western Svecofennian orogen, central Sweden: constraints from U/Pb zircon and titanite geochronology. *Precambrian Research*, **161**(3–4), 250–278. https://doi.org/10.1016/j.precamres.2007.08.008

Huhma, H. 1986. Sm–Nd, U–Pb and Pb–Pb isotopic evidence for the origin of the early Proterozoic Svecokarelian crust in Finland. *Geological Survey of Finland, Bulletin*, **337**.

Huhma, H., Mänttäri, I., Peltonen, P., Kontinen, A., Halkoaho, T., Hanski, E. et al. 2012. The age of the Archaean greenstone belts in Finland. *Geological Survey of Finland Special Paper*, **54**, 74–175.

Jansson, N. F. and Allen, R. L. 2011. Timing of volcanism, hydrothermal alteration and ore formation at Garpenberg, Bergslagen, Sweden. *GFF*, **133**(1–2), 3–18. https://doi.org/10.1080/11035897.2010.547597

Kara, J., Väisänen, M., Johansson, Å., Lahaye, Y., O'Brien, H. and Eklund, O. 2018. 1.90-1.88Ga arc magmatism of central Fennoscandia: geochemistry, U-Pb geochronology, Sm-Nd and Lu-Hf isotope systematics of plutonic-volcanic rocks from southern Finland. *Geologica Acta*, **16**(1), 1–23. https://doi.org/10.1344/GeologicaActa2018.16.1.1

Kara, J., Väisänen, M., Heinonen, J. S., Lahaye, Y., O'Brien, H. and Huhma, H. 2020. Tracing arclogites in the Paleoproterozoic Era – a shift from 1.88 Ga calc-alkaline to 1.86 Ga high-Nb and adakite-like magmatism in central Fennoscandian Shield. *Lithos*, **372–373**, 105663. https://doi.org/10.1016/j.lithos.2020.105663

Kara, J., Leskelä, T., Väisänen, M., Skyttä, P., Lahaye, Y., Tiainen, M. and Leväniemi, H. 2021. Early Svecofennian rift-related magmatism: geochemistry, U–Pb–Hf zircon isotope data and tectonic setting of the Au-hosting Uunimäki gabbro, SW Finland. *Precambrian Research*, **364**, 106364. https://doi.org/10.1016/j.precamres.2021.106364

Kara, J., Väisänen, M. and O'Brien, H. 2022. Zircon dating of the basalt and felsic dyke in Haveri, SW Finland. *Bulletin of the Geological Society of Finland*, **94**(2), 109–118. https://doi.org/10.17741/bgsf/94.2.001

Kirkland, C. L., Fougerouse, D., Reddy, S. M., Hollis, J. and Saxey, D. W. 2018. Assessing the mechanisms of common Pb incorporation into titanite. *Chemical Geology*, **483**, 558–566. https://doi.org/10.1016/j.chemgeo.2018.03.026

Kohn, M. J. 2017. Titanite petrochronology. *Reviews in Mineralogy and Geochemistry*, **83**(1), 419–441. https://doi.org/10.2138/rmg.2017.83.13

Kohonen, J., Lahtinen, R., Luukas, J. and Nironen, M. 2021. Classification of regional-scale tectonic map units in Finland. *Geological*

Survey of Finland, Bulletin, **412**, 33–80. https://doi.org/10.30440/bt412.2

Lahtinen, R., Korja, A. and Nironen, M. 2005. Paleoproterozoic tectonic evolution. In *Precambrian Geology of Finland – Key to the Evolution of the Fennoscandian Shield* (Lehtinen, M., Nurmi, P. A. and Rämö, O. T., eds). Elsevier, Amsterdam, 481–531. https://doi.org/10.1016/S0166-2635(05)80012-X

Laitala, M. 1994. Lohja. *Geological map of Finland 1:100 000: pre-Quaternary rocks, sheet 2041*. Geological Survey of Finland, Espoo.

Latvalahti, U. 1979. Cu-Pb-Zn ores in the Aijala-Orijärvi area, southwest Finland. *Economic Geology*, **74**(5), 1035–1059. https://doi.org/10.2113/gsecongeo.74.5.1035

Ludwig, K. R. 2003. *User's Manual for Isoplot 4.15. A Geochronological Toolkit for Microsoft Excel*. Berkley Geochronology Center Special Publication, No. 4.

Marillo-Sialer, E., Woodhead, J., Hanchar, J. M., Reddy, S. M., Greig, A., Hergt, J. et al. 2016. An investigation of the laser-induced zircon 'matrix effect'. *Chemical Geology*, **438**, 11–24. https://doi.org/10.1016/j.chemgeo.2016.05.014

Miller, C. F., McDowell, S. M. and Mapes, R. W. 2003. Hot and cold granites? Implications of zircon saturation temperatures and preservation of inheritance. *Geology*, **31**(6), 529–532. https://doi.org/10.1130/0091-7613(2003)031<0529:HACGIO>2.0.CO;2

Müller, W., Shelley, M., Miller, P. and Broude, S. 2009. Initial performance metrics of a new custom-designed ArF excimer LA-ICPMS system coupled to a two volume laser-ablation cell. *Journal of Analytical Atomic Spectrometry*, **24**, 209–214. https://doi.org/10.1039/B805995K

Nironen, M. 2017a. Guide to the geological map of Finland – bedrock 1: 1 000 000. *Geological Survey of Finland Special Paper*, **60**, 41–76.

Nironen, M. 2017b. The Salittu Formation in southwestern Finland, part II: picritic-basaltic volcanism in mature arc environment. *Bulletin of the Geological Society of Finland*, **89**, 5–19. https://doi.org/10.17741/bgsf/89.1.001

Nironen, M., Mänttäri, I. and Väisänen, M. 2016. The Salittu Formation in southwestern Finland, part I: structure, age and stratigraphy. *Bulletin of the Geological Society of Finland*, **88**(2), 85–103. https://doi.org/10.17741/bgsf/88.2.003

Ploegsma, M. and Westra, L. 1990. The Early Proterozoic Orijärvi triangle (southwest Finland): a key area on the tectonic evolution of the Svecofennides. *Precambrian Research*, **47**(1–2), 51–69. https://doi.org/10.1016/0301-9268(90)90030-T

Reinikainen, J. 2001. Petrogenesis of Paleoproterozoic marbles in the Svecofennian domain, Finland. *Geological Survey of Finland, Report of Investigations*, **154**.

Rutanen, H., Andersson, U. B., Väisänen, M., Johansson, Å., Fröjdö, S., Lahaye, Y. and Eklund, O. 2011. 1.8 Ga magmatism in southern Finland: strongly enriched mantle and juvenile crustal sources in a post-collisional setting. *International Geology Review*, **53**(14), 1622–1683. https://doi.org/10.1080/00206814.2010.496241

Salli, I. 1955. *Suomusjärvi. Geological map of Finland 1:100 000: pre-Quaternary rocks, sheet 2023*. Geological Survey of Finland, Espoo.

Salminen, P. E. and Kurhila, M. 2023. New age constraints for metasedimentary rocks in southern Finland. *Bulletin of the Geological Society of Finland*, **95**(2), 83–106. https://doi.org/10.17741/bgsf/95.2.001

Schreurs, J. and Westra, L. 1986. The thermotectonic evolution of a Proterozoic, low pressure, granulite dome, West Uusimaa, SW Finland. *Contributions to Mineralogy and Petrology*, **93**, 236–250. https://doi.org/10.1007/BF00371326

Schreurs, J., van Kooperen, P. and Westra, L. 1986. Ultramafic metavolcanic rocks of early Proterozoic age in West-Uusimaa, SW Finland. *Neues Jahrbuch für Mineralogie Abhandlungen*, **155**, 185–201.

Schumacher, J. C. and Czank, M. 1987. Mineralogy of triple- and double-chain pyriboles from Orijärvi, southwest Finland. *American Mineralogist*, **72**(3–4), 345–352.

Selonen, O., Ehlers, C. and Lindroos, A. 1996. Structural features and emplacement of the late Svecofennian Perniö granite sheet in southern Finland. *Bulletin of the Geological Society of Finland*, **68**(2), 5–17. https://doi.org/10.17741/bgsf/68.2.001

Skyttä, P., Käpyaho, A. and Mänttäri, I. 2005. Supracrustal rocks in the Kuovila area, southern Finland: structural evolution, geochemical characteristics and the age of volcanism. *Bulletin of the Geological Society of Finland*, **77**(2), 129–150. https://doi.org/10.17741/bgsf/77.2.003

Skyttä, P., Väisänen, M. and Mänttäri, I. 2006. Preservation of Palaeoproterozoic early Svecofennian structures in the Orijärvi area, SW Finland – evidence for polyphase strain partitioning. *Precambrian Research*, **150**(3–4), 153–172. https://doi.org/10.1016/j.precamres.2006.07.005

Soesoo, A., Nirgi, S. and Plado, J. 2020. The evolution of the Estonian Precambrian basement: geological, geophysical and geochronological constraints. *Transactions of the Karelian Research Centre of the Russian Academy of Sciences*, **2**, 18–33. https://doi.org/10.17076/geo1185

Spandler, C., Hammerli, J., Sha, P., Hilbert-Wolf, H., Hu, Y., Roberts, E. and Schmitz, M. 2016. MKED1: a new titanite standard for in situ analysis of Sm–Nd isotopes and U–Pb geochronology. *Chemical Geology*, **425**, 110–126. https://doi.org/10.1016/j.chemgeo.2016.01.002

Torvela, T. and Kurhila, M. 2022. Timing of syn-orogenic, high-grade transtensional shear zone formation in the West Uusimaa Complex, Finland. *Bulletin of the Geological Society of Finland*, **94**(1), 5–22. https://doi.org/10.17741/bgsf/94.1.001

Väisänen, M. and Kirkland, C. L. 2008. U-Th-Pb zircon geochronology on igneous rocks in the Toija and Salittu Formations, Orijärvi area, southwestern Finland: constraints on the age of volcanism and metamorphism. *Bulletin of the Geological Society of Finland*, **80**(2), 73–87. https://doi.org/10.17741/bgsf/80.2.001

Väisänen, M. and Mänttäri, I. 2002. 1.90–1.88 Ga arc and back-arc basin in the Orijärvi area, SW Finland. *Bulletin of the Geological Society of Finland*, **74**(1–2), 185–214. https://doi.org/10.17741/bgsf/74.1-2.009

Väisänen, M. and Westerlund G. 2007. Palaeoproterozoic mafic and intermediate metavolcanic rocks in the Turku area, SW Finland. *Bulletin of the Geological Society of Finland*, **79**(2), 127–141. https://doi.org/10.17741/bgsf/79.2.001

Väisänen, M., Mänttäri, I. and Hölttä, P. 2002. Svecofennian magmatic and metamorphic evolution in southwestern Finland as revealed by U–Pb zircon SIMS geochronology. *Precambrian Research*, **116**(1–2), 111–127. https://doi.org/10.1016/S0301-9268(02)00019-0